Universidad de Investigación de Tecnología Experimental Yachay

Escuela de Ciencias Físicas y Nanotecnología

TÍTULO: Griffiths phase and nontrivial collective behavior in dynamical networks

Trabajo de integración curricular presentado como requisito para la obtención del título de Físico

Autor:
Juan Sebastián Velez Rojas

Tutor:
Mario Cosenza, PhD.

Urcuquí - Noviembre, 2023

AUTORÍA

Yo, **Velez Rojas Juan Sebastián**, con cédula de identidad **1105652935**, declaro que las ideas, juicios, valoraciones, interpretaciones, consultas bibliográficas, definiciones y conceptualizaciones expuestas en el presente trabajo; así cómo, los procedimientos y herramientas utilizadas en la investigación, son de absoluta responsabilidad de el/la autor(a) del trabajo de integración curricular. Así mismo, me acojo a los reglamentos internos de la Universidad de Investigación de Tecnología Experimental Yachay.

Urcuquí, Noviembre del 2023.

Juan Sebastián Velez Rojas
CI: 1105652935

AUTORIZACIÓN DE PUBLICACIÓN

Yo, **Velez Rojas Juan Sebastián**, con cédula de identidad **1105652935**, cedo a la Universidad de Investigación de Tecnología Experimental Yachay, los derechos de publicación de la presente obra, sin que deba haber un reconocimiento económico por este concepto. Declaro además que el texto del presente trabajo de titulación no podrá ser cedido a ninguna empresa editorial para su publicación u otros fines, sin contar previamente con la autorización escrita de la Universidad.

Asimismo, autorizo a la Universidad que realice la digitalización y publicación de este trabajo de integración curricular en el repositorio virtual, de conformidad a lo dispuesto en el Art. 144 de la Ley Orgánica de Educación Superior

Urcuquí, Noviembre del 2023.

Juan Sebastián Velez Rojas
CI: 1105652935

Dedication

To the irreplaceable engines that keep me going—*my family: Karina, Vicente, Emilio, Katty, Jose Luis, Mirian, Pastor, Inti, and Kaleb*—I can't wait to get us all under one big residence, a place each of us can call our home.

Acknowledgements

Siempre he creído que el limitado espacio-tiempo de una simple hoja de papel jamás podría contener la vasta magnitud de mi gratitud hacia ustedes. Sin embargo, permítanme intentarlo aquí:

- A mi madre, cuyo amor incondicional, consejos, escucha y paciencia hacia mí no dejará de dar frutos.
- A mi pa, tu sabiduría en momentos críticos es un tesoro que no cambiaría por nada en este mundo.
- A José, Emy, Katty, Pastor, Mirian, Inti, sus perspectivas de la vida las porto en mi pecho a dondequiera que vaya.
- A mis panas, Antonio, Ricardo, Pablo, Jean, conectar con ustedes desde el primer día que empezó este viaje, sin siquiera saber de dónde venimos y a dónde vamos, no tiene nombre.
- A Arianna, por hacerme consciente de todo con su inigualable empatía.
- A Diana, por tu habilidad para expresarme lo obvio y mostrarme el valor del autocuidado.
- Al profesor José Luis Herrera, quien me ayudó computacionalmente a entender las redes complejas.
- A Ricardo Velasco, tu aporte computacional y resiliencia fueron extremadamente útiles.
- A CEDIA, el acceso gratuito a su clúster es como tener un laboratorio abierto 24/7. A mi hijo/a le enseñaré a usar el clúster.
- A Antonio Villagómez, por mantener la vigilia en la escritura de esta tesis.
- A los Caóticos, por ser una fuente inagotable de ideas valiosas y por hacerme cultivar la paciencia.
- A COSSY, por ser un claro ejemplo de fenómeno emergente con un sistema de individuos extraordinarios.
- A LANET, por motivarme a mantenerme curioso y disciplinado mediante las personas fabulosas que conocí.
- A los profesores Henry, Wladimir, Mayra, su motivación por la física y cada detalle detrás es un elixir.
- Al profesor Orlando, por transmitirme el carácter y carisma inherentes a sus organizaciones.
- A Yachay, por brindarme la oportunidad de cruzar caminos con gente excepcional como Mateo, Jordan, Gabriela, Emily, Brandon, Marcos, Stephanie, Shirley, Yomaira, Pauly, David E, Javier C, Sebastián N, Juan Diego, Víctor, Lizbeth, Esteban, Julio, Arturo, Guido, Jerry, María Belen, María Jose A, Francis, Gilda, profesora Clara y muchos más.
- A Kuhiniko Kaneko, Giorgio Parisi, Roger Penrose, Olaf Sporns, John Beggs, Miguel Ángel Muñoz, Edgar Roldán, científicos indescriptibles, quizá hasta genios, pero por sobre todo altamente motivantes con sus aportes científicos. Estoy seguro de que algún día tendré la fortuna de colaborar con ustedes.
- A los que no podré colaborar pero sí mantener la llama de la ciencia, como: Richard Feynman, Stephen Hawking, Albert Einstein, Per Bak, Leonardo da Vinci.
- Al fenomeno emergente llamado vida y darme la conciencia de considerarme afortunado de ser quien soy.

Y en especial al Profesor Mario Cosenza, por ser un observador imparcial de cada una de mis ideas no triviales, por más locas que sean; tus anécdotas, consejos y conocimientos los llevaré eternamente. Esta tesis nace de diálogos con el Profesor Mario sobre la interpretación de la vida y la muerte a través de los sistemas complejos: '¿Qué transición existe entre los estados de la vida y la muerte?'

Resumen

Investigamos la aparición del novedoso fenómeno de la fase caótica de Griffiths en redes de mapas acoplados. En esta fase, la distribución de tamaños de clusters dinámicos sincronizados sigue una ley de potencia, no sólo en un valor crítico de un parámetro, sino en un amplio intervalo de parámetros. Buscamos los mecanismos subyacentes que pueden dar lugar a una fase caótica de Griffiths en redes de mapas caóticos mediante el uso de diferentes funciones dinámicas. Encontramos que surge una fase caótica de Griffiths en redes que poseen dinámicas basadas en neuronas; apoyando así el punto de vista de que esta fase puede jugar un papel relevante en el comportamiento crítico observado en los sistemas neuronales y en la dinámica del cerebro. Introducimos una cantidad estadística que mide la dispersión. de clusters para caracterizar la fase caótica de Griffith en redes dinámicas. Empleamos una medida de heterogeneidad para caracterizar la dispersión de los parámetros de los mapas locales. Descubrimos que la heterogeneidad, ya sea en la topología de la red o los parámetros de los elementos dinámicos, es un ingrediente esencial para la emergencia de la phase caótica de Griffiths.

Palabras clave: Redes de mapas acoplados, fase caótica de Griffiths, Sistemas Complejos, Fenómenos Críticos, Clustering Dinámico.

Abstract

We investigate the occurrence of the novel phenomenon of chaotic Griffiths phase in coupled map networks. In this phase, the distribution of sizes of synchronized clusters follows a power law, not just at a critical value of a parameter, but on a broad range of parameters. We search for the underlying mechanisms that can give rise to a chaotic Griffiths phase in a coupled chaotic map networks by using different map dynamics. We find that a chaotic Griffiths phase appears in networks possessing neuron-based dynamics; thus supporting the view that this phase can play a relevant role in the critical behavior observed in neural systems and brain dynamics. We introduce a statistical quantity that measures the dispersion of clusters in order to characterize the chaotic Griffith phase in dynamical networks. We employ a heterogeneity measure to characterize the dispersion of the parameters of the local maps. We unveil that heterogeneity in either the network topology or in the parameters of the dynamical elements are crucial ingredients for the emergence of the chaotic Griffiths phase.

Keywords: Coupled Map Networks, Chaotic Griffiths Phase, Complex Systems, Brain Criticality, Dynamical Clustering.

Contents

1 Introduction **21**
- 1.1 Research problem . . . 22
- 1.2 Objectives . . . 22
  - 1.2.1 General objectives . . . 22
  - 1.2.2 Specific objectives . . . 22

2 Theoretical framework **23**
- 2.1 Phase Transitions . . . 23
- 2.2 Griffiths Phase . . . 23
- 2.3 Brain Criticality . . . 26
- 2.4 Griffiths Phase in Brain Dynamics . . . 29
- 2.5 Chaotic Griffiths Phase . . . 29

3 Griffiths Phase: Our Findings **33**
- 3.1 Mechanisms of Emergence of Chaotic Griffiths Phase . . . 33
  - 3.1.1 Mechanism 1: Random Network Topology. . . . 33
  - 3.1.2 Mechanism 2: Heterogeneity in Parameters. . . . 35
  - 3.1.3 Mechanism 3: Simultaneous Random Network and Parameter Heterogeneity. . . . 38
- 3.2 Measures behind criticality . . . 39
  - 3.2.1 Power Law . . . 39
  - 3.2.2 Dispersion of Fraction of Clusters (DFC) . . . 46
  - 3.2.3 Asymmetry Measure . . . 53
  - 3.2.4 Small World Network . . . 56

4 Conclusions **61**

Bibliography **63**

Appendices **68**

A Codes in Python **71**
  - A.0.1 Power Law Clusters Counting . . . 71

List of Figures

2.1 Sketch of a diluted magnet. The shaded region is devoid of impurities and therefore acts as a piece of the clean bulk system. Picture taken from[1] 24

2.2 Illustration of a coexistence of phases. Notice heterogeneity between two states: Trees and grasses. Each graph change according model competition between young trees a_{est}, control parameter fix $b_{max} = 1$, which is possible temporal correlations in weather. Picture taken from[2] 25

2.3 Sketch of an lattice with Spins pointing up and down randomly. Picture taken from[3] 26

2.4 Graph of the phases of Ising model with spin down as gray color and spin up as white color. Image taken from[3] 27

2.5 a) Image of a two-dimensional Ising model at T_c. Notice the predominance of large black or white regions. Figure adapted from[3]. b) Sketch of Power Law: By measuring both the size and frequency of each cluster, we observe a signature of scale invariance. 27

2.6 Experiment draft of Neuronal Avalanches in Neocortical Circuits. a) Measure of size and frequency of neurons. b) Size of avalanches composed by neurons. Picture taken from[4]. 28

2.7 Size distributions for avalanches follow power laws independently of bin width Δt. A, Probability distribution of avalanche sizes (number of electrodes activated) in log-log coordinates at different Δt (average for $n = 7$ cultures). The linear part of each function indicates power law. Picture extracted from[5]. 28

2.8 Time Series of States $x_{2t}(i)$:Evolved over an Erdös–Rényi network $A_{i,j}$ of $N = 100$ nodes, using n as the discrete time variable. States are plotted every two steps. Initial transients excluded are 10^5 steps. The phase is generated by parameters $a = 1.7$ and $N = 200$. In specific, a) $\epsilon = 0.5, k = 20$ (phase(ii)). b) $\epsilon = 0.35, k = 15$ (phase(iii)). c) $\epsilon = 0.2, k = 10$ (phase(iv)). d) $\epsilon = 0.05, k = 10$ (phase(v)). Phase diagram of the CMN with $a = 1.7$ and $N = 200$. Each phase (i)-(v) (see text) is determined by the Lyapunov exponents. The configuration of the phase diagram is independent of a, while the phase boundary is shifted. Both figures are obtained from[6] 30

2.9 The distribution $P(s)$ of cluster size s. Log-log plot. $a = 1.7, k = 20$, and $N = 16384$. The results from $\epsilon = 0.45, 0.475, 0.5, 0.525, 0.55, 0.575$, and 0.6 are plotted with different colors. The distribution is obtained by sampling over 10^3 steps, with 100 initial conditions, over 100 networks, by using the threshold $\delta = 10^{-3}$, while the exponents do not vary as long as this threshold is sufficiently small, and also the network sample dependence is negligible. The figure is taken from[6] 30

3.1 *Time Series of States $X_{2t}(i)$ within Griffith's Chaotic Phase:* Evolved over an Erdös–Rényi network $A_{i,j}$ of $N = 1000$ nodes, using t as the discrete time variable. States are plotted every two steps. Initial transients excluded are 10^5 steps. The phase is generated by parameters $\epsilon = 0.5$, $a = 1.7$ and $k = 20$. 34

3.2 a) Bifurcation map of the quadratic equation: States $x(i)$ are plotted for a values between 1.0 and 2.0. The chaotic range [1.6, 2.0] is marked with red dotted lines. b) Time series of states $x_{2t}(i)$ within Griffith's Chaotic Phase are generated using a Global Coupled Map with $N = 10^4$ nodes. Each node has a randomly assigned a_i value in the range $[1.6, 2.0]$. The time variable t is discrete, and states are plotted every two steps. The coupling parameter is $\epsilon = 0.38$, and initial transients of 10^5 steps are excluded. 36

3.3 a) Bifurcation map of the logarithmic function: We plot states against the control parameter b, ranging from -1.5 to 1.5. Red dotted lines mark the chaotic range $[-1.0, 1.0]$. b) Time series in Griffith's Chaotic Phase: Generated using a Global Map Network with $N = 10^3$ nodes. Each node has a randomly assigned b_i value in the range $[-1.0, 1.0]$. The time variable t is discrete, and states are plotted every two steps. Initial transients of 10^5 steps are excluded, and the coupling parameter is $\epsilon = 0.7$. 37

3.4 Network Heterogeneity Illustration: A single Chialvo Neuron Map over time is plotted using the parameters $a = 0.89$, $c = 0.28$, $b = 0.18$, and $k = 0.027$. The brain illustration is created in Python using NetworkX. . 37

3.5 a) Bifurcation diagram for the Chialvo Neuron Map: We plot states against the parameter k, ranging from 0.02 to 0.035. The chaotic range $k_i \in [0.026, 0.03]$ is marked with red dotted lines. b) Time Evolution in Griffith's Chaotic Phase: Using a Global Coupled Map with $N = 10^3$ nodes, we plot states $X_t(i)$ over discrete time t. Initial transients of 10^5 steps are excluded. The phase is generated with coupling $\epsilon = 0.12$ and parameters $a = 0.89$, $b = 0.18$, $c = 0.28$. Each node has a randomly assigned k_i value in the range $k_i \in [0.026, 0.03]$. 38

3.6 Temporal series of states $X_t(i)$ for an Erdös–Rényi network (Mechanism 1) with $N = 10^3$ nodes and an average of $k = 20$ neighbors. The discrete time variable t is used, and the first 10^5 transient steps are excluded. The phase is generated with a coupling constant $\epsilon = 0.21$ and parameters $a = 0.89$, $b = 0.18$, $c = 0.28$. For Mechanism 2, each node is assigned a k_i value, uniformly and randomly distributed in the range $[0.026, 0.03]$. 39

3.7 Temporal evolution of the maximal cluster size: $a = 1.7, k = 20$, and $N = 1000$. The cluster is computed by using the threshold $\delta = 10^{-3}$, while this intermittent behavior does not vary as long as it is sufficiently small. $\epsilon = 0.5$ (blue line), $\epsilon = 0.55$ (green line) $\epsilon = 0.6$ (red line), in the chaotic Griffiths phase[6]. 40

3.8 The distribution $P(s)$ of cluster size s. Log-log plot. $a = 1.7, k = 20$, and $N = 16384$. The results from $\epsilon = 0.45, 0.475, 0.5, 0.525, 0.55, 0.575$, and 0.6 are plotted with different colors. The distribution is obtained by sampling over 10^3 steps, with 100 initial conditions, over 100 networks, by using the threshold $\delta = 10^{-3}$, while the exponents do not vary as long as this threshold is sufficiently small, and also the network sample dependence is negligible. Figure is taken from[6]. 41

3.9 Time Series of Maximum Cluster Size: The data is generated from a Global Coupled Network with $N = 1000$ nodes, each assigned a parameter a_i in the range $[1.6, 2.0]$. The bin size used for the plot is $\delta = 10^{-4}$. Different colored lines represent varying coupling strengths: $\epsilon = 0.35$, $\epsilon = 0.4$, and $\epsilon = 0.5$, all of which fall within the chaotic Griffith's Phase. 42

3.10 **Power Law Distribution**: In this log-log plot, we examine cluster size distribution ($(F(s))$) within a globally coupled network of $N = 16,000$ nodes which operate with heterogeneity $a_i \in [0.026, 0.03]$. Three coupling strengths ($\epsilon = 0.35, 0.4$, and 0.45) are represented by distinct colors. Data is from 20 networks observed over 10^3 steps, using a cluster-counting bin size of $\delta = 10^{-4}$. Exponents α are calculated with Python's `powerlaw` library, sensitive to ϵ. 43

3.11 **Time Series of Maximum Cluster Size.** The data is generated from Globally Coupled Network of $N = 1000$ nodes, each assigned a parameter $k_i \in [0.026, 0.03]$. The bin size used for the plot is $\delta = 10^{-5}$. Different colored lines represent varying coupling strengths: $\epsilon = 0.12$, $\epsilon = 0.18$, and $\epsilon = 0.27$, all within the chaotic Griffith's Phase. 43

3.12 Power Law Distribution. We analyze the distribution $F(s)$ of cluster sizes s using a log-log plot. Data comes from a globally coupled Chialvo Neuron Maps with $N = 16000$ nodes. Each node with $k_i \in [0.026, 0.03]$ uniformly and randomly assigned. We present results for three different coupling strengths—$\epsilon = 0.12, 0.15$, and 0.2—each distinguished by color. The data is aggregated from 20 unique networks and observed over 10^3 steps. We use a bin size of $\delta = 10^{-5}$ for cluster counting. The exponent α, is calculated using Python's `powerlaw` library. 44

3.13 a) Time Series of Maximum Cluster Size. The data is obtained from an Erdös–Rényi network consisting of 1000 nodes with an average of K=20 neighbors. Each node is assigned a parameter k_i that follows a uniform random distribution in the range of [0.026 to 0.03]. The bin size for the plot is set to $\delta = 20^{-5}$. The different colored lines on the graph represent various coupling strengths ϵ: 0.2, 0.25, and 0.3. All of these values fall inside the chaotic Griffith's Phase. b) Similar to (a), but with a bin size of $\delta = 10^{-5}$. . . . 45

3.14 Power Law Distribution. In the Log-Log plot, we examine the distribution $F(s)$ of cluster sizes s in a Erdös–Rényi network of $N = 10000$ nodes. Each node operates with the Chialvo Neuron Map, with k_i parameters uniformly distributed im range [0.026, 0.03]. We present results for three different coupling strengths—$\epsilon = 0.15, 0.2$, and 0.25—each distinguished by color. The data is compiled from 20 unique networks, each observed over 10^3 steps. We employ a cluster-counting bin size of $\delta = 10^{-5}$. The exponent α is computed using Python's `powerlaw` library. 45

3.15 Fraction of Clusters: The plot displays the variable p_t calculated over different time series corresponding to $\epsilon = 0.05$ (black line), 0.13 (red line), and 0.55 (blue line). These values of ϵ represent varying degrees of interaction in a Globally Coupled Chialvo Neuron Map system with $N = 1000$. Parameters are set as $a = 0.89$, $b = 0.18$, $c = 0.28$, and k ranges from 0.026 to 0.03. Labels on the plot indicate collective states: D.P for Desynchronization Phase, G.P for chaotic Griffith's Phase, and S.P for Synchronization Phase. . . 46

3.16 Dispersion of Fraction of Clusters (DFC). Plotted as a function of the coupling constant ϵ over the range [0.05, 0.9], divided into 100 uniform steps. A bin size of 10^{-3} is used in the DFC for cluster identification. Calculations are performed for a Erdös–Rényi network of $N = 100$ nodes with $a = 1.7$ and $K = 20$. Averages for DFC are taken over 20 realizations, each with 10^5 transients discarded and uniformly random initial conditions in range $[0, 1]$. Labels indicate collective states: G.P for Griffith's Phase, S.P for Synchronization Phase and O.P for Other Phases. Dotted black lines represent limits according the time series. 47

3.17 Dispersion of Fraction of Clusters (DFC): The plot shows the normalized DFC as a function of the coupling constant ϵ, ranging from 0.05 to 0.9. This is based on a Global Coupled network of $N = 100$ nodes, each node with a parameter $a_i \in [1.6, 2.0]$. DFC is averaged over 20 runs, disregarding the first 10^5 steps in each run. A bin size of 10^{-3} is used in the DFC for cluster identification. Initial node conditions are uniformly distributed between 0 and 1. Labels such as *O.P*, *G.P*, and *S.P* indicate Other Phases, Griffith's Phase, and Synchronization Phase, respectively. Dotted black lines mark time-series-based limits. 48

3.18 Time series of Global Coupled Quadratic Map. Order Phase at $\epsilon = 0.33$, Synchronization Phase at $\epsilon = 0.8$, and, at the peak of DFC with $\epsilon = 0.38$ belonging to the Griffith's Phase. All observations are made with $N = 100$ nodes, employing correspondence mechanism 2, detailed in 3.1.2. 48

3.19 Dispersion of Fraction of Clusters (DFC): The normalized DFC is plotted as a function of the coupling constant ϵ, which varies from 0.05 to 1. Counted states comes from Global Coupled Logarithmic Maps with $N = 100$ nodes, each assigned a randomly parameter $b_i \in [-1, 1]$. The DFC values are averaged over 20 networks, each discarding the first 10^5 transient steps and using uniformly random initial conditions in the range $[0, 1]$. A bin size of 10^{-3} is employed for counting clusters. We note each phase, D.P, "G.P", and S.P represent Desynchronization, "Griffiths", and Synchronization Phases. 49

3.20 Time series for Global Coupled Logarithmic Maps reveal distinct phases: Desynchronization Phase at $\epsilon = 0.2$, "Griffiths Phase" at $\epsilon = 0.6$, and Synchronization Phase at $\epsilon = 0.96$. Data is from a $N = 100$-node network governed by mechanism 2, detailed in Section 3.1.2 50

3.21 Dispersion of Fraction of Clusters (DFC): The normalized DFC is plotted as a function of ϵ, ranging from 0.05 to 0.9. The data is derived from Global Coupled Maps with $N = 100$ nodes, each assigned a randomly parameter uniformly distributed in the range $k_i \in [0.026, 0.03]$. DFC is averaged over 20 runs, omitting the first 10^5 steps with different initial conditions [0,1]. A bin size of 10^{-3} is used for DFC. Labels O.P, G.P, and S.P signify Other, Griffiths, and Synchronization Phases, respectively. 50

3.22 Time series for Global Coupled Chialvo Maps are presented for three distinct phases: The Chimera Phase at $\epsilon = 0.08$, the Synchronization Phase at $\epsilon = 0.5$, and the Griffith's Phase at the DFC peak with $\epsilon = 0.11$. All data are collected from a network of $N = 100$ nodes, in accordance with mechanism 2, as developed in Section 3.1.2. 51

3.23 Dispersion of Fraction of Clusters: The plot illustrates the metric DFC in blue as a function of ϵ, spanning from 0.05 to 0.9. Calculations are based on a Global Coupled Maps of $N = 100$ nodes, each with a local parameter k_i in the range $[0.026, 0.027]$. DFC is averaged over 20 runs with initial conditions taken in range [0,1], and omitting the first 10^5 steps. A bin size of 10^{-3} is used for measure DFC. Labels O.P, G.P, and S.P signify Other Phases, Griffiths Phase, and Synchronization Phase. 51

3.24 The plot displays the Dispersion of Fraction of Clusters (DFC), illustrated in blue, as a function of ϵ which ranges from 0.05 to 0.9. The calculations are performed on an Erdös–Rényi Network with $N = 100$ nodes and an average of $K = 20$ neighbors per node. Each node has a local parameter k_i within the range $[0.026, 0.03]$. The DFC values are averaged over 20 runs, disregarding the initial 10^5 steps. A bin size of 10^{-3} is employed for DFC. The labels signify O.P: Other Phases, G.P: Griffiths Phase, and S.P: Synchronization Phase. 52

3.25 The time series describes a notable peak in our measure, marking three distinct phases: the Desynchronization at $\epsilon = 0.05$, the Synchronization Phase at $\epsilon = 0.16$, and the Griffith's Phase at the peak of DFC with $\epsilon = 0.6$. All data are collected from a network of $N = 100$ nodes using correspondence mechanism 2. 52

3.26 Dispersion of Fraction of Clusters (DFC) in blue, as a function of ϵ that varies from 0.05 to 0.9. The analysis is based on an Erdös–Rényi Network with $N = 100$ nodes and an average of $K = 20$ neighbors per node. Each node has a local parameter k_i in the range $[0.026, 0.027]$. DFC values are averaged over 20 runs, omitting the initial 10^5 steps. A bin size of 10^{-3} is used for DFC. Labels such as O.P., G.P., and S.P. stand for Other Phases, Griffiths Phase, and Synchronization Phase, respectively. 53

3.27 The Dispersion of Fraction of Clusters (DFC) is plotted against the asymmetry parameter A for globally coupled quadratic maps consisting of $N = 100$ nodes with heterogeneity $a_i \in [1.6, 2.0]$, as specified in Equations 3.3. The coupling constant is set at $\epsilon = 0.41$. This plot is generated from 20 realizations. . . . 54

3.28 The plot displays the Dispersion of Fraction of Clusters (DFC) as a function of the asymmetry parameter A. It is based on globally coupled Logarithmic maps with $N = 100$ nodes and each node heterogeneity $b_i \in [0, 1]$, as outlined in Equations 3.4. The coupling constant is set at $\epsilon = 0.61$, and the data is derived from 20 different realizations. 54

3.29 The plot shows the Dispersion of Fraction of Clusters (DFC) against the asymmetry parameter A. It uses globally coupled Chialvo maps with $N = 100$ nodes, each having a heterogeneity parameter k_i in the range $[0.026, 0.03]$, as specified in equations 3.5. The coupling constant is fixed at $\epsilon = 0.12$, and the plot includes data from 20 different realizations. 55

3.30 Dispersion of Fraction of Clusters (DFC) as a function of the asymmetry parameter A. It is based on Chialvo Networks coupled through an Erdös–Rényi topology with $N = 100$ nodes and an average of $K = 20$ neighbors per node. Each node has a heterogeneity parameter k_i in the range $[0.026, 0.03]$, as described in Equations 3.5. The coupling constant is set at $\epsilon = 0.17$, and the data is derived from 20 different realizations. 56

3.31 The figure depicts the rewiring process guided by parameter p in a Network. At $p = 0$, the network is regular; at $p = 1$, it becomes random. Intermediate values of p represents an Small World Network. Illustration taken from[7]. 56

3.32 Clustering (in blue) and Path Length (in orange) are plotted as functions of the parameter p. X-axis is in log-scale. N=100, K=40 averaged over 30 samples, a red dotted line marks the network configuration we will use, with a rewiring parameter set at $p = 0.038$. 57

3.33 The plot showcases DFC in blue as a function of ϵ, spanning from 0 to 1. Calculations are based on a Small World Network of $N = 100$ nodes with p=0.038 and K = 40 (mean number of neighbours), each with a local parameter k_i in the range $[0.026, 0.03]$. DFC is averaged over 20 runs, omitting the first 10^5 steps. A bin size of 10^{-3} is used for DFC. acronyms D.P, G.P, and S.P stand for Desynchronization, Griffiths, and Synchronization Phases, respectively. 58

3.34 The time series of three distinct phases: the Desynchronization Phase at $\epsilon = 0.1$, the Griffith's Phase at the peak of DFC with $\epsilon = 0.2$, and Synchronization Phase at $\epsilon = 0.7$. All data are collected from a network of $N = 100$, $K = 40$ and $p = 0.038$ guided by Equations 3.5 58

3.35 a) Time Series of $x(i)$: Sourced from a Small World Network with specifications $N = 100$, $K = 40$, and $p = 0.038$, as dictated by Equations 3.5. We consider k_i in the interval [0.026, 0.03] and exclude the first 10^5 transient steps. The coupling constant is $\epsilon = 0.17$. b) Similar to a), but uniquely differentiated by an interaction parameter $\epsilon = 0.2$ and a time frame of [0,100]. 59

Chapter 1

Introduction

In recent years there has been much interest in the study of the collective behavior of networks of coupled dynamical units as models of complex systems. A complex system is a system of interactive elements whose collective behavior cannot be inferred from the knowledge of the behavior of its constituent elements[8,9]. The concept of complex system has become a new paradigm for the search for a unified interpretation of the mechanisms for the emergence of structures, patterns, and functionality in a variety of natural and technological systems. Complex systems have been found to possess universal characteristics, independently of their context. The investigation of the interrelationships between the constituent elements in complex systems has revealed the existence of underlying connectivity which also have universal properties[10].

Synchronization is the simplest and more abundant form of collective behavior arising in systems of interacting elements[11]. Synchronization occurs when all the elements in the system share the same state sustained in time, i.e., the elements reach a common time evolution. Spontaneous or autonomous synchronization can take place without the presence of external fields or driving forces. Synchronization is widely observed in nature; from coupled pendulum clocks, firing of fireflies, the motion of schools of fish, flying flocks, swarms of birds, bees evading predators, in the periodic clapping of hands of people in a stadium, people walking on bridges, social consensus, or in epileptic seizures. It has also been investigated for technological applications, including wind turbines, satellite clocks, or electrical power lines[11].

If the dynamic elements on the network are responsible for some function, synchronization would imply the loss of the functionality. In the power grid network, such synchronization may lead to a global black out[12,13], while in neural networks, it may lead to the loss of cognitive function. In contrast, global synchronization is not common in biological systems, although they involve dynamics with many degrees, which are often suggested to lie at a critical state, represented by a power law of activities[14–20].

In this context, coupled map lattices or coupled map networks (CMN) have provided useful models for the study of diverse processes in complex systems, with the advantage of being computationally efficient. Coupled map networks (CMN) are spatio-temporal dynamical systems where space and time are discrete, but the dynamical states are continuous. They consist of a set of maps or iterative functions considered as nodes interacting on a lattice or on a general network[21].

In particular, coupled maps on networks (CMN) are relevant for exploring the collective behaviors in high-dimensional systems, where conditions for chaotic synchronization[22,23] and splitting of elements into a few synchronized clusters, which also depends on network structures[24–29], have been investigated. However, the collective dynamics arising between synchronization and desynchronization is not well known yet and constitutes an open problem.

In 2016, K Kaneko and his student K. Shinoda discovered a novel intermediate phase between synchronization and disorder in a chaotic coupled map network, where the elements intermittently evolve between synchronization and desynchronization[6]. They called this state "chaotic Griffiths phase". In this phase, distribution of sizes of synchronized clusters was found to follow power law, not just at a critical value, but on a broad range of a parameter. This behavior is reminiscent of a Griffiths phase found in Ising models of ferromagnets[30]. Furhermore, Kaneko and Shinoda at the end of their paper suggest that the chaotic Griffiths phase may provide an alternative view on the critical states observed in biological networks, especially in brain dynamics as correlation of neural activities [18,19,31,32]. In fact, it has been reported that the conscious brain spends long intervals of time in a critical state [18,31,33]

1.1 Research problem

Motivated by the above suggestion and observations, in this Thesis we investigate the occurrence of chaotic Griffiths phase in coupled map networks possessing neuron-based dynamics. A chaotic Griffiths phase appearing in such systems will bring support to the view that this phase can play a relevant role in the criticality observed in neural systems and brain dynamics. We search for the underlying mechanisms that can give rise to a chaotic Griffiths phase in a coupled chaotic map networks by using different map dynamics. We introduce a statistical quantity to measure the dispersion of clusters in order to characterize the chaotic Griffith phase in dynamical networks. We employ a heterogeneity measure to characterize the dispersion of the parameters of the local maps. We investigate the role of heterogeneity in either the network topology or in the parameters of the dynamical elements on the emergence of the chaotic Griffiths phase.

1.2 Objectives

1.2.1 General objectives

Understand the mechanisms that lead to the emergence of the chaotic Griffiths phase in dynamical networks.

1.2.2 Specific objectives

1. Show the generality of the phenomenon of chaotic Griffiths phase in coupled map networks by investigating different map functions.
2. Characterize the statistical properties of the chaotic Griffiths phase in coupled map networks through a general measure.
3. Investigate the emergence of chaotic Griffiths phase in coupled map networks possessing neuron-based dynamics.
4. Study the influence of the heterogeneity in the network connections on the occurrence of the chaotic Griffiths phase in coupled map networks.
5. Study the influence of heterogeneity in the parameters of the local elements on the emergence of the chaotic Griffiths phase in coupled map networks.

Chapter 2

Theoretical framework

2.1 Phase Transitions

In our universe, there exist phenomena that challenge our fundamental understanding of states in nature. One such enigma is the occurrence of phase transitions. The concept of a phase transition is clear in our everyday experiences—water boiling into steam or ferromagnetic materials changing to paramagnetic. In general, there are first-order transitions, also called explosive synchronization, where the order parameter changes discontinuously, the main examples of these transitions are matter changing from its states of liquid, solid, and gas and expansion of the universe[34]. However, complexity and universality of phase transitions become apparent when one delves into the realm of second-order transitions. This are characterized by a continuous change whose distribution satisfies a Power Law, accompanied by high correlation length[3,35,36].

From the perspective of statistical physics, there are significant questions behind these phenomena. A substantial path to answers has been joined by Leo Kadanoff, in which he formalized the universality classes of systems behind each second order phase transition[37]. Specifically, he found that phenomena with the same Beta exponent belong to the same class. According to Giorgio Parisi, this can lead to a Platonic view of nature having few classes according to their exponents, and each universality class representing an Idea[3]. Ultimately, the Beta exponent will depend on the degrees of freedom of your system[37].

Relevant formalism in the study of phase transitions came at the hands of Kenneth Wilson, in which he developed the "Renormalization Group" (RG)[38], a formalism that allows for the calculation of critical exponents. In simple terms, renormalization allows us to transition from one scale to another, consequently maintaining a consistent representation at each scale. It takes advantage of the fact that the system at the mesoscopic (intermediate) level is scale-invariant.

Interestingly, Giorgio Parisi and Kenneth discussed the importance of these exponents in 1971 at a conference in Rome:

G: "The information on the value of the critical exponents is in the first Feynman diagrams."

K: "I know that; the problem is how to extract it."

This conversation took place before the revolutionary method of RG[3].

2.2 Griffiths Phase

Robert B. Griffiths was the pioneer to question the phenomena of first-order phase transitions within a simple ferromagnet[30]. This investigation led to the discovery of the influence of rare regions. These regions are expansive spatial areas remarkably free from impurities, illustrated in Figure 2.1. Despite the larger system is in a paramagnetic state, these isolated regions exhibit a localized magnetic order[1].

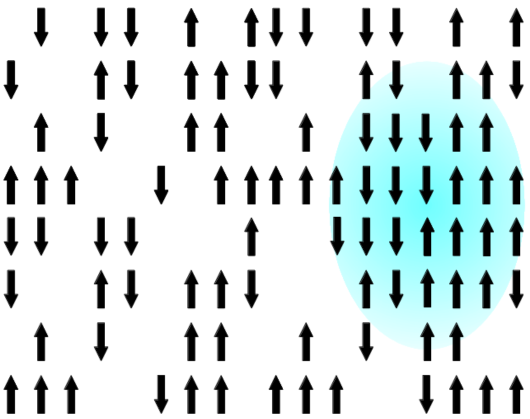

Figure 2.1: Sketch of a diluted magnet. The shaded region is devoid of impurities and therefore acts as a piece of the clean bulk system. Picture taken from[1]

Intriguingly, rare regions serve for the emergence of singularities in the free energy of the system. Such singularities, now termed Griffiths singularities. In specific, it is defined

Griffiths Phase: Main characteristic 1

It is defined as the specific temperature interval $T_c < T < {T_c}^0$ characterized by the presence of singularities in the free energy of the system, known as Griffiths singularities.[1,39,40].

It is worth noting that analogous singularities are also observable on the other side of the phase transition. Griffiths phase appears in systems with quenched disorder. This type of quenched disorder is sometimes referred to as 'weak' disorder[1]. Quenched disorder is a general characteristic of the system, while rare regions are specific areas within the system where the effects of quenched disorder become particularly significant. The central focus lies on the simplest category of disorder capable of inducing spatial variations in the coupling strength. This disorder is well known to induce non-trivial critical phases in systems[1,30,41]. In such phases, exponentially rare regions survive for exponentially large times, generating a phase with generic power-law behavior.[1].

Griffiths Phase: Main characteristic 2

Power-law scaling is a signature of Griffiths Phase, appearing in multiple contexts such as the mean lifetime of systems, rare regions or clusters size distribution maintaining for large times.

Several studies have explored the concept of rare regions in other context in order to confirm the presence of Griffiths Phases (GP)[2,33,42–45]. In these studies, one salient observation is that in single-variable (or mean-field) models of stochastic populations, the introduction of environmental noise alters the mean lifetime of the system—defined as the time required to reach an absorbing state—from an exponential function to a power-law function of the system size[46,47].

With these motivations, investigators extend into the realm of spatially extended systems, going beyond mean-field approximations. Here, the role of temporal disorder, which takes the role of quenched disorder, is explored. The findings reveal a specific region in the active phase of systems with absorbing states and fluctuating external conditions, termed the "temporal Griffiths phase," where the mean lifetime exhibits generic power-law scaling[43].

Temporal Griffiths Phases (TGPs) share profound similarities with the standard GP. However, the roles of space and time are intriguingly reversed. In standard GPs, spatial disorder leads to algebraic scaling as a function of time, whereas in TGPs, temporal disorder results in similar scaling as a function of system size[43].

Temporal Griffiths Phase

The Temporal Griffiths Phase (TGP) is a specific region in the active phase of systems with absorbing states and fluctuating external conditions. In this phase, the mean lifetime of the system exhibits generic power-law scaling.

One particularly illuminating example that elucidates the universality of Griffiths Phase is the "savanna problem"[2], which explores the long-term coexistence of trees (state 1) and grasses (state 2) without one outcompeting the other, see Figure 2.2. A minimal stochastic model incorporating both spatial disorder and temporal randomness provides a theoretical framework that induces the presence of generic power laws in the active phase. This active phase, when influenced by time-disorder, is remarkably stable in the large N limit, obtaining the designation of a "temporal Griffiths phase." This offers a theoretical framework for the observed stability in dynamical phase coexistence. In essence, this model shows that the only requirement for dynamical phase coexistence is fluctuating external conditions[2].

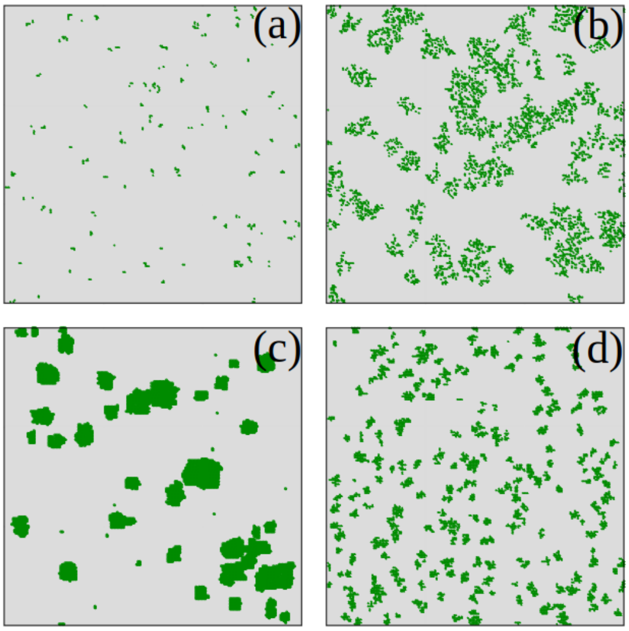

Figure 2.2: Illustration of a coexistence of phases. Notice heterogeneity between two states: Trees and grasses. Each graph change according model competition between young trees a_{est}, control parameter fix $b_{max} = 1$, which is possible temporal correlations in weather. Picture taken from[2]

Another important study focuses on complex networks[42]. Investigators comprehend that disorder effects seem similar in both equilibrium and non-equilibrium states. Rare-region effects transcend the frontier between equilibrium and nonequilibrium. They study the simplest epidemic model, the Quenched Contact Process (QCP), on Erdös–Rényi (ER) random networks. The results confirm that quenched disorder can induce GPs and other rare-region effects, leading to generic slow dynamical processes on ER networks[42].

Griffiths Phase: Main characteristic 3

In the study of Griffiths Phases, slow dynamical processes are a recurring theme. This is due to the fact that rare regions exhibit slow dynamics, as flipping them needs a coherent change of the order parameter over a wide area[1].

2.3 Brain Criticality

> “Inside our heads is a magnificent structure that controls our actions and somehow evokes an awareness of the world around” —Roger Penrose, *The Emperor’s New Mind*

In nature, the phenomenon known as criticality occurs during second-order transitions[4]. This is a domain that exists in a curious region —between the order and the disorder, between the periodicity and the randomness of a chaotic system. These fascinating transitions have long captivated scientists because of their universality[4]. Abundant evidence indicates that some of the most fascinating phenomena of living systems –such as memory or problem solving skills– emerge from the collective that can operate near critical points[48]. Similar cases have been observed in a variety of contexts such as the optimal growth of cells[16] , bacterial clustering[49], gene expression patterns[14], the flocking behavior of birds[50], and even societal interactions[51]. Intriguingly, all these complex behaviors often arise from rather simple underlying equations or rules[50]. Now, let us delve into the universal characteristics that typify systems operating at a critical point. One of the most salient features is the emergence of different phases. Specifically, when a system is in a critical phase, small changes can generate dramatic large-scale consequences[50]. This is closely related to the generation of singularities in the system’s energy function, defined in Box 2.2. To elucidate the concept of criticality, one might consider the Ising model, first proposed by Ernst Ising in his doctoral thesis[3]. This model simplifies the complexities in order to understand reality by considering only two possible states of spin: up and down. As represented in Figure 2.3.

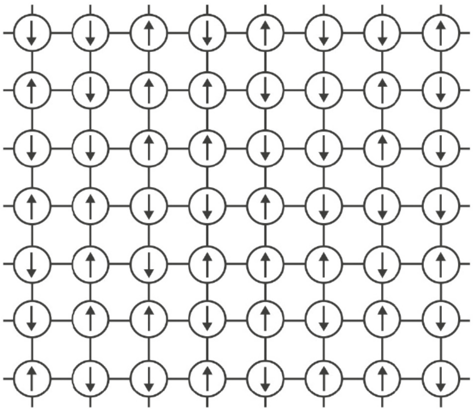

Figure 2.3: Sketch of an lattice with Spins pointing up and down randomly. Picture taken from[3]

In the ordered state, or what is termed the ’ferromagnetic phase,’ the majority of spins align in a single direction. On the other hand, in the disordered state, known as the ’paramagnetic phase,’ spins are evenly split—50% up, 50% down, all randomly oriented[3]. Illustrated in Figure 2.4.

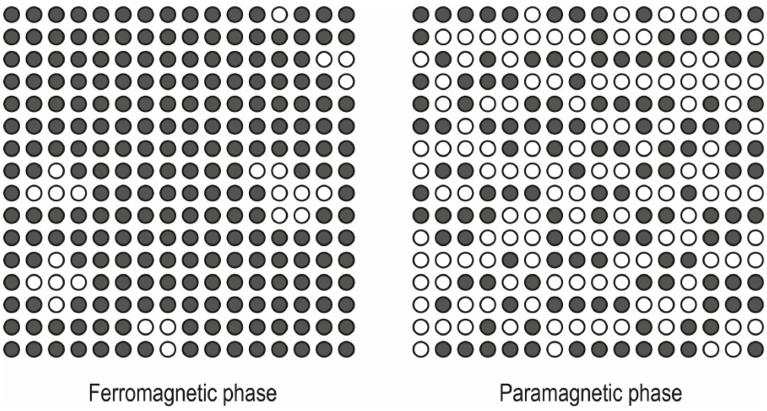

Figure 2.4: Graph of the phases of Ising model with spin down as gray color and spin up as white color. Image taken from[3]

Temperature acts as the control parameter in this model. Within the critical point T_c, it governs the transition between two distinct states, consider a) Figure 2.5. When we examine the size and frequency of clusters—known as rare regions—we observe a fascinating property called scale invariance, which[3] is represented in b) Figure 2.5.

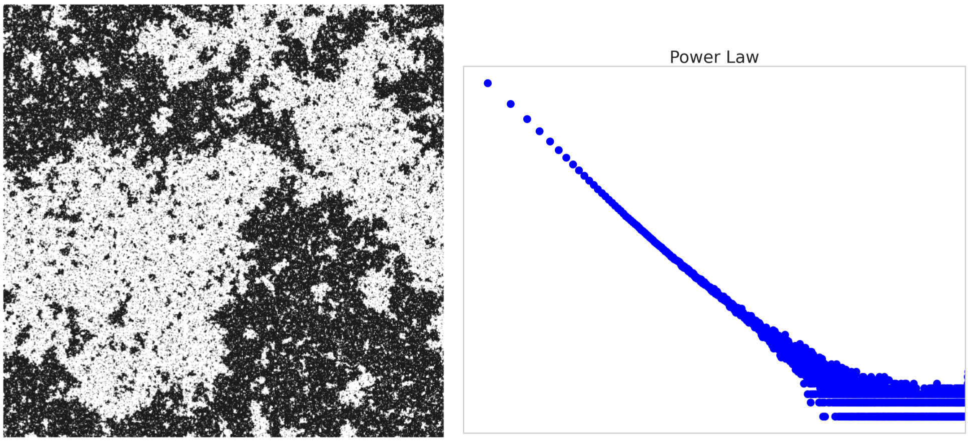

Figure 2.5: a) Image of a two-dimensional Ising model at T_c. Notice the predominance of large black or white regions. Figure adapted from[3]. b) Sketch of Power Law: By measuring both the size and frequency of each cluster, we observe a signature of scale invariance.

Power-law distributions are common in various fields, from earthquakes and solar flares[52–54] to biological systems[52,55,56]. This scale-invariance is often described as 'self-similarity' or 'scale-free'[35]. Within this context, the laws of physics remain consistent across all scales. One way to understand this is through correlation measures. In stable states—either ordered or disordered—interaction correlations are low. However, at critical points, these correlations peak[35], implying that a single spin influence are able to extend indefinitely[36]. Per Bak has offered a compelling perspective on this, introducing the concept of Self-Organized Criticality (SOC)[50]. His work delineates a crucial difference: SOCs criticality is not the same as the critical points in equilibrium systems, which require parameter tuning. In their study, criticality in dynamical systems serves as an attractor reached from non equilibrium states. This inherent feature eliminates the necessity for fine-tuning to attain scale invariance in nature[57]. Turning to the brain, a marvelously complex network composed of 10^{11} neurons and 10^{15} synapses[58–61], we find that neuron activity becomes especially significant in the critical phase due to high correlation properties. In this phase, even a minor input can trigger what we might call a 'thought,' manifesting as an avalanche[50]. This concept has been improved over time[32,62–65], suggesting that the brain must operate in a critical state to adapt to a somewhat critical world[32]. Additionally, the brain's interaction with its environment also shows scale-invariant features[5,66,67]. One pioneer experiment, in which researchers isolate young gray matter cortex and allow it to grow. Measurements of neuron cluster sizes reveal a power-law distribution, with each cluster representing an 'avalanche'. This can be appreciated in Figure 2.6

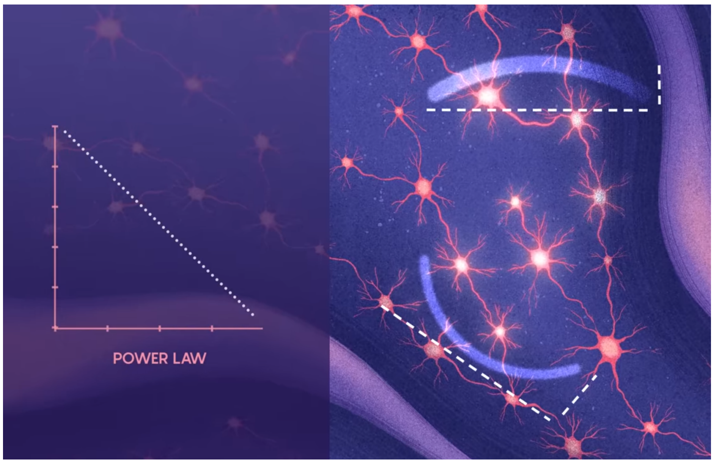

Figure 2.6: Experiment draft of Neuronal Avalanches in Neocortical Circuits. a) Measure of size and frequency of neurons. b) Size of avalanches composed by neurons. Picture taken from[4].

This property is crucial for brain dynamics, as it enables interactions across the entire network[35]. This 'scale-free' nature ensures that a single neuron could probably influence the entire cortical region[35]. Such a state allows the brain to preserve, maximize, and transmit information over extended periods[59,62,68]. Deviations from this critical state are often indicative of diseases[67]. Oficial result from this experiment is showed in Figure 2.7

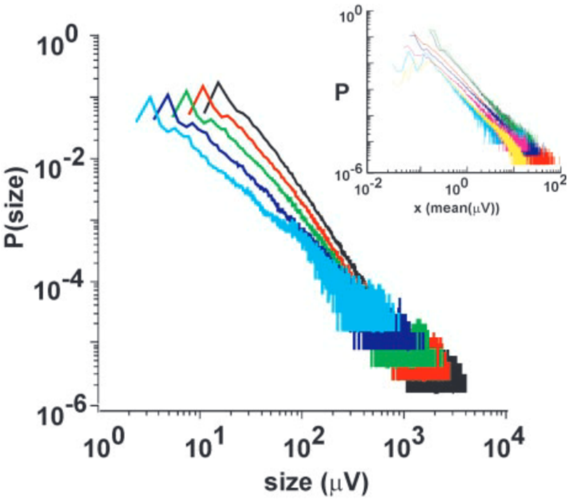

Figure 2.7: Size distributions for avalanches follow power laws independently of bin width Δt. A, Probability distribution of avalanche sizes (number of electrodes activated) in log-log coordinates at different Δt (average for $n = 7$ cultures). The linear part of each function indicates power law. Picture extracted from[5].

2.4 Griffiths Phase in Brain Dynamics

Recent papers have expanded our understanding of brain dynamics by examining complex networks. One such study[33] draws from fMRI data of the human brain at rest, suggesting that brain activity hovers around an extended region near a critical point, rather than at a single critical point[69]. This implies that cortical networks operate in a broader region around the critical point[33,61,70].

Pioneering research has also explored the role of hierarchical-modular networks (HMN) in critical dynamics[33,59,71,72]. These studies employ a mix of analytical and computational tools to map anatomical connections in the human brain. They find that the hierarchical and modular structure of the brain induces a Griffiths phase (GP), not just in stylized models but also in real neural networks like those in C. elegans and the human connectome[33].

Another line of research focuses on the collective aspects of brain function. Specifically, the brain capabilities arise from the collective interactions of neurons[73,74]. These studies aim to identify universal features of whole-brain connectivity and dynamics, such as:

- **Resting-State Networks:** Long-term fMRI data reveals that spontaneous activity in different brain regions is correlated, forming resting-state networks (RSN)[61,75,76].
- **Structural Networks:** Networks of the brain are organized in a hierarchical-modular manner[33,61,71] and feature a core-periphery structure with connector hubs.
- **Segregation and Integration:** The brain processes different types of input in segregated regions, which are then integrated for advanced cognitive functions[59,61,77].
- **Criticality and Griffiths Phases:** It is proposed that the concept of criticality can be extended by incorporating Griffiths phases[33,61]. These phases appear in systems with structural heterogeneity and are characterized by "frustrated synchronization"[61,78,79].

Finally, these studies explore the interplay between structure and dynamics to understand the Griffiths Phase. They use simple structural networks and minimal dynamics models, like the Kuramoto model, to study neuronal interactions. The key takeaway is that large variability in brain activity can occur in regions corresponding to Griffiths-like phases, where transient levels of synchrony are observed[61].

2.5 Chaotic Griffiths Phase

In 2016, Kunihiko Kaneko and K. Shinoda introduced the concept of Chaotic Griffiths Phase as collective state emerging in Coupled Map Networks (CMN)[6]. This research explores the diverse modeling possibilities of CMN, including the emergence of collective phases that have macroscopic relevance. For example, global synchronization in neural networks could lead to cognitive dysfunction. CMN models, which are characterized by many degrees of freedom, often suggest the emergence of a critical state, characterized by a power law[6,18–20].

Consider the general expression for a CMN[6]:

$$x_{n+1}(i) = (1-\epsilon) f\left(x_n(i)\right) + \frac{\epsilon}{k_i} \sum_{j=1}^{N} A_{i,j} f\left(x_n(j)\right) \tag{2.1}$$

Here, $A_{i,j}$ represents the connections or the adjacency matrix of the network and local dynamics is given by the map $f(x_n(i))$. The coupling strength is denoted by ϵ, and k_i represents the number of neighbors for each node. Shinoda and Kaneko considered an Erdös–Rényi network and a local logistic map $f(x_n) = 1 - a(x_n)^2$, with $a = 1.7$ to ensure chaos.

By varying the coupling strength ϵ, several dynamical collective phases emerge.

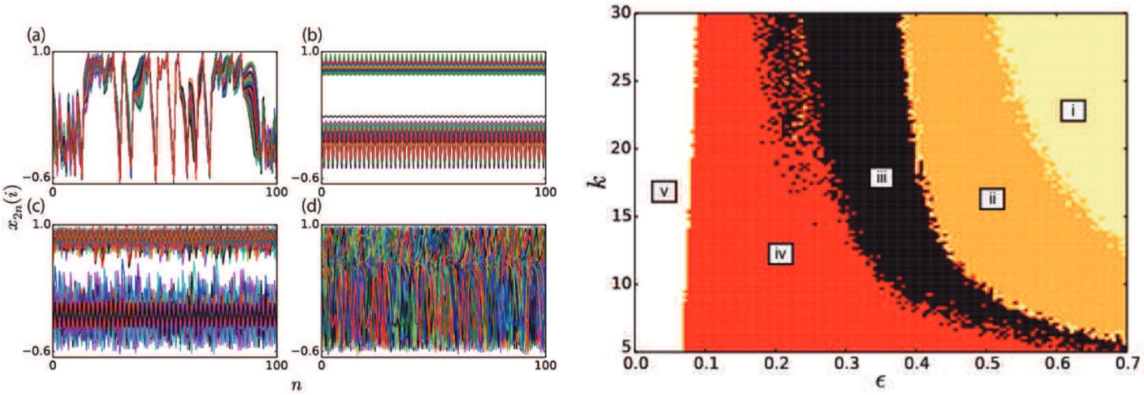

Figure 2.8: Time Series of States $x_{2t}(i)$:Evolved over an Erdös–Rényi network $A_{i,j}$ of $N = 100$ nodes, using n as the discrete time variable. States are plotted every two steps. Initial transients excluded are 10^5 steps. The phase is generated by parameters $a = 1.7$ and $N = 200$. In specific, a) $\epsilon = 0.5, k = 20$ (phase(ii)). b) $\epsilon = 0.35, k = 15$ (phase(iii)). c) $\epsilon = 0.2, k = 10$ (phase(iv)). d) $\epsilon = 0.05, k = 10$ (phase(v)). Phase diagram of the CMN with $a = 1.7$ and $N = 200$. Each phase (i)-(v) (see text) is determined by the Lyapunov exponents. The configuration of the phase diagram is independent of a, while the phase boundary is shifted. Both figures are obtained from[6]

Specifically, the Chaotic Griffiths Phase (CGP) is of interest because it is unique to network systems and does not have an equivalent in other topologies like Coupled Map Lattices (CML) or Global Coupled Maps (GCM). In CGP, synchronized clusters spontaneously form and dissolve, exhibiting a power-law size distribution and anomalous Lyapunov spectra.

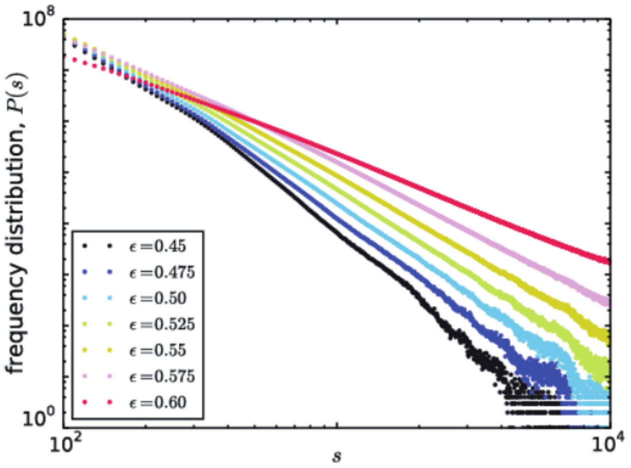

Figure 2.9: The distribution $P(s)$ of cluster size s. Log-log plot. $a = 1.7, k = 20$, and $N = 16384$. The results from $\epsilon = 0.45, 0.475, 0.5, 0.525, 0.55, 0.575$, and 0.6 are plotted with different colors. The distribution is obtained by sampling over 10^3 steps, with 100 initial conditions, over 100 networks, by using the threshold $\delta = 10^{-3}$, while the exponents do not vary as long as this threshold is sufficiently small, and also the network sample dependence is negligible. The figure is taken from[6]

Contrasting this phase with other Griffiths Phases discussed in this thesis, it's crucial to highlight that global synchronization is not an absorbing state in our system. Instead, the power-law behavior manifests as a chaotic attractor. This distinction justifies its label as Chaotic Griffiths Phase[6].

Towards the end of Shinoda and Kaneko's paper, they suggest that the Chaotic Griffiths Phase may have significance in the realm of brain dynamics. This idea, coupled with the Brain Criticality Section 2.3, prompts us to delve deeper into the study of this fascinating phenomenon.

Chapter 3

Griffiths Phase: Our Findings

I outline the structure of this research, designed to offer a clear understanding of the phenomena in question, as follows:

1. **Mechanisms of Emergence**: We will explore various mechanisms, that induce critical regions in Coupled Map Networks. Each mechanism will be illustrated with a time-series graph for improve comprehension.
2. **Measures of Criticality**: Rigorous metrics are essential for confirming criticality. We will introduce various measures to better understand this region. Additionally, we will present our unique measure, Dispersion of the Fraction of Clusters (DFC), which identifies criticality based on the size of clusters in time-series data.

3.1 Mechanisms of Emergence of Chaotic Griffiths Phase

One way to see the universality of the results is testing over several most used dynamics maps. Then, we shall focus on three distinct maps, each offering unique intrinsic properties and rich implications for the realm of physics:

- **Quadratic Map**: This is a one-dimensional map known for its period-doubling bifurcations, stable phases, and chaotic regions that have periodic windows. The quadratic and logistic maps are said to be “conjugate,” meaning they behave similarly in terms of dynamics.[80]
- **Logarithmic Map**: This map doesn’t fit into the usual categories of unimodal or bounded maps. It has neither a maximum nor a minimum. The bifurcation map shows that there are no distinct chaotic bands for any value of a parameter $b \in [-1, 1]$.[81]
- **Chialvo Map[82]**: This is a two-dimensional map with excitable dynamics, as discussed in section 3.1.2

To better understand these mechanisms, we follow Leo Kadanoff’s idea that the exponent Beta depends on the degrees of freedom of the system[37]. Then, each of these mechanisms increases the system’s degrees of freedom, and curiously, give rise to critical regions, most notably the Griffith’s Chaotic Phase. The underlying connections among these observations remain an open question.

3.1.1 Mechanism 1: Random Network Topology.

> “There is an old debate," Erdös liked to say, "about whether you create mathematics or just discover it. In other words, are the truths already there, even if we don’t yet know them?" Erdös had a clear answer to this question: Mathematical truths are there among the list of absolute truths, and we just rediscover them. Random graph theory, so elegant and simple, seemed to him to belong to the eternal truths. Yet today we know that random networks played little role in assembling our universe."

— Albert-László Barabási, 2002

The first objective of our study is to replicate the phenomenon of the Griffiths Chaotic Phase, as initially discovered by K.Shinoda and Kunihiko Kaneko.[6]

Main characteristics

In essence, the key features of this mechanism are:

Table 3.1: Key Features of Mechanism 1

Feature	**Description**
Topology	Random. Erdös–Rényi topology.
Parameters in Local Dynamics	Homogeneous. We set $a = 1.7$.

Model

We focus on a Coupled Map Network governed by Erdös–Rényi topology and chaotic quadratic maps in each node. Specifically, we examine the following coupled map network equation[6]:

$$x_{t+1}(i) = (1-\epsilon)f\left(x_t(i)\right) + \frac{\epsilon}{k_i}\sum_{j=1}^{N} A_{i,j} f\left(x_t(j)\right) \tag{3.1}$$

In this study, the local dynamics for each node are described by $x(t+1) = 1 - a(x_t)^2$, representing the quadratic map. We set $a = 1.7$ to ensure chaotic behavior in the quadratic map. The coupling strength is denoted by ϵ. The adjacency matrix $A_{i,j}$ corresponds to an Erdös–Rényi random network, and k_i is the degree of node i, with an average degree of K. Varying ϵ and K introduces instability and gives rise to nontrivial dynamics[6].

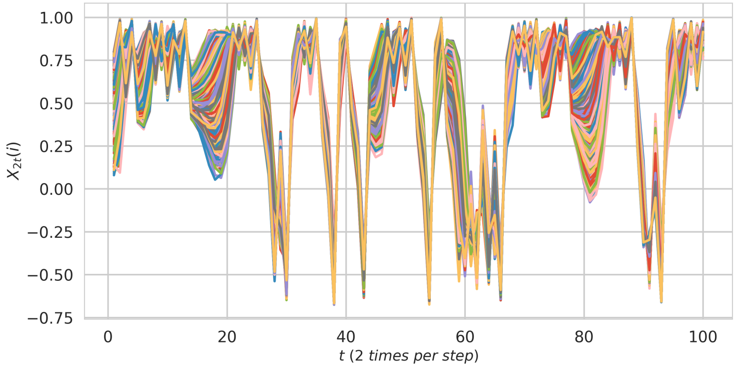

Figure 3.1: *Time Series of States $X_{2t}(i)$ within Griffith's Chaotic Phase:* Evolved over an Erdös–Rényi network $A_{i,j}$ of $N = 1000$ nodes, using t as the discrete time variable. States are plotted every two steps. Initial transients excluded are 10^5 steps. The phase is generated by parameters $\epsilon = 0.5$, $a = 1.7$ and $k = 20$.

Notions

- To enhance the clarity of the phenomena, the states considered will advance in steps of $2t$ instead of t. This is because the quadratic map naturally exhibits a period-two oscillation.

- This mechanism produces the Griffiths Chaotic Phase (GCP) only for quadratic maps, not for logarithmic or Chialvo maps. One hypothesis suggests that this phenomenon occurs due to the inherent characteristics intrinsic to the family of unimodal maps.

3.1.2 Mechanism 2: Heterogeneity in Parameters.

> "The most universal property in a life system is high-dimensional diversity."
>
> — Kunihiko Kaneko, 2023, ICTP in Trieste

Our central hypothesis comes from a body of literature that underscores the benefits of heterogeneity over homogeneity in various systems[83].

- **Collective Behaviors:** Research indicates that heterogeneity can enhance regularity in collective dynamics and induce collective behaviors[84,85].
- **Social Networks:** Zhou et al. (2020) found that heterogeneity in social status can drive network evolution towards self-optimization[86].
- **Networks of the Brain[59]:** In his insightful work, Olaf Sporns elaborates on Ashby's "Law of Requisite Variety" from 1956, a principle that serves as a main ingredient for understanding heterogeneity of systems[87]. The law establishes that a system's internal diversity response must match the heterogeneity of environmental perturbations to maintain stability. Yaneer Bar-Yam further generalized this concept, proposing a trade-off between the diversity of system responses and the scales at which these responses are coordinated.

In our research, we extract this complex concept to its essence. We focus on the role of heterogeneity in control parameters, specifically within the chaotic domain delineated by the bifurcation map governing local dynamics.

Main characteristics

Table 3.2: Key Features of Mechanism 2

Feature	**Description**
Topology	Global Coupling Network.
Parameters in Local Dynamics	Heterogeneous. We have set the chaotic range of a, b and k.

Model

To validate the contributions of Mechanism 2, we employ a network of Global Coupled Maps (GCM) system. This choice serves to enhance the clarity and effectiveness of our approach. The equation for this system is[88]:

$$x_{t+1}(i) = (1-\epsilon) f\left(x_t(i)\right) + \frac{\epsilon}{N}\sum_{j=1}^{N} f\left(x_t(j)\right) \tag{3.2}$$

where $x_t(i)$ denotes the state of the i-th node element ($i \in \{1, \ldots, N\}$) at a discrete temporal instance t. Here, ϵ serves as the coupling parameter, and f encapsulates the local dynamics of each element. Importantly, the division by N in the second term implies an averaging over all elements. This equation indicates the dynamical coupling in which each node will evolve[88].

Quadratic Map:

The local dynamics for each node is governed by the equation[80]:

$$f(x) = 1 - a(x)^2 \tag{3.3}$$

For our study, we assign a heterogeneous value of a to each node, denoted as a_i, which falls within the range $1.6 \leq a_i \leq 2.0$. This ensures that the system exhibits chaotic dynamics.

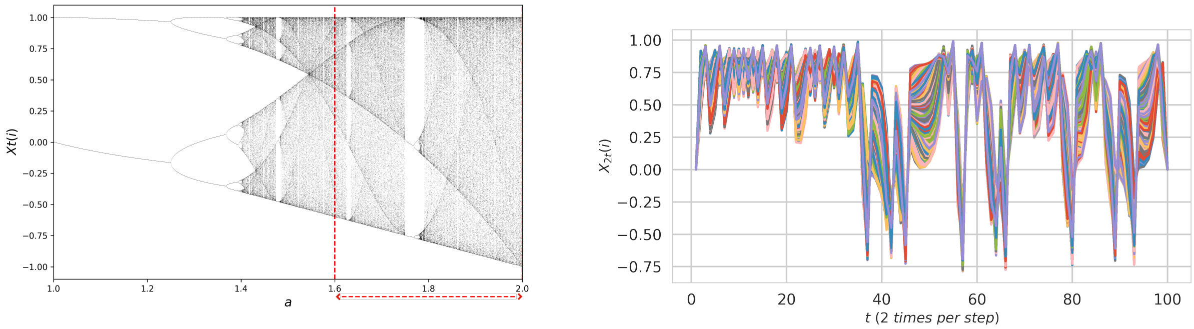

Figure 3.2: a) Bifurcation map of the quadratic equation: States $x(i)$ are plotted for a values between 1.0 and 2.0. The chaotic range [1.6, 2.0] is marked with red dotted lines. b) Time series of states $x_{2t}(i)$ within Griffith's Chaotic Phase are generated using a Global Coupled Map with $N = 10^4$ nodes. Each node has a randomly assigned a_i value in the range $[1.6, 2.0]$. The time variable t is discrete, and states are plotted every two steps. The coupling parameter is $\epsilon = 0.38$, and initial transients of 10^5 steps are excluded.

Notions

- The representation aims to clarify the chaotic range we are using. This case includes some periodic windows.

Logarithmic Map:

The local dynamics corresponds to the logarithmic map[81],

$$x_{t+1} = f(x_t) = b + \ln |x_t| \tag{3.4}$$

For consistency, we select the parameter b_i to lie within the range $-1.0 \leq b \leq 1.0$, which corresponds to the chaotic robust.

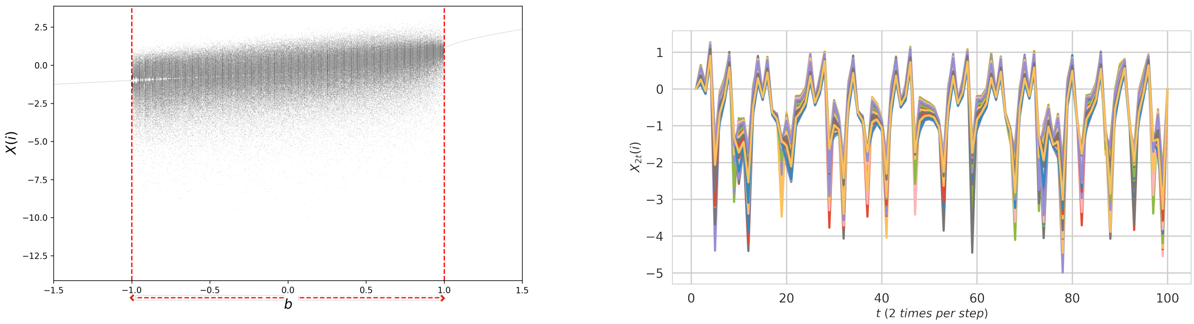

Figure 3.3: a) Bifurcation map of the logarithmic function: We plot states against the control parameter b, ranging from -1.5 to 1.5. Red dotted lines mark the chaotic range $[-1.0, 1.0]$. b) Time series in Griffith's Chaotic Phase: Generated using a Global Map Network with $N = 10^3$ nodes. Each node has a randomly assigned b_i value in the range $[-1.0, 1.0]$. The time variable t is discrete, and states are plotted every two steps. Initial transients of 10^5 steps are excluded, and the coupling parameter is $\epsilon = 0.7$.

Chialvo Neuron Map:

Mathematically, we describe excitable dynamics by using this two equations[82]:

$$\begin{aligned} x_{t+1} &= f(x_t, y_t) = x_t^2 \exp(y_t - x_t) + k, \\ y_{t+1} &= g(x_t, y_t) = a y_t - b x_t + c, \end{aligned} \tag{3.5}$$

the variable x serves as the activation or potential, while y functions as a recovery-like variable. The subscript t marks discrete time steps, indicating the system's temporal evolution. The model incorporates four parameters—a, b, c, and k—to induce system instability. Notably, k can function as either a constant bias or a time-dependent additive perturbation.

To get a clear idea of this heterogeneity. We will follow 3.1.2 concept inside Chialvo Map equations:

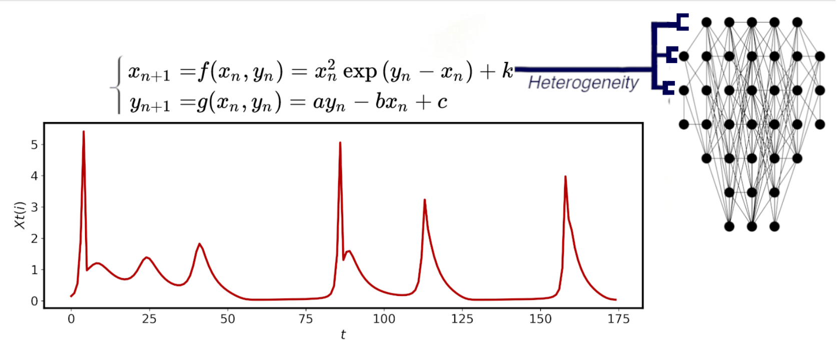

Figure 3.4: Network Heterogeneity Illustration: A single Chialvo Neuron Map over time is plotted using the parameters $a = 0.89$, $c = 0.28$, $b = 0.18$, and $k = 0.027$. The brain illustration is created in Python using NetworkX.

As depicted in Figure 3.4, each node responds differently based on its individual time series and the parameter k. We introduce variability in k within the chaotic range $[0.026, 0.03]$, which preserves the neuron's behavior[82]. By coupling a large number of nodes using Mechanism 2 and the Chialvo Neuron equations, we obtain:

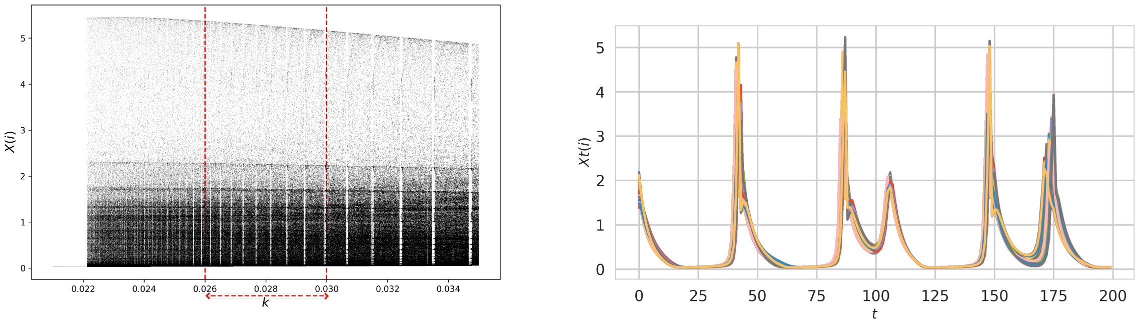

Figure 3.5: a) Bifurcation diagram for the Chialvo Neuron Map: We plot states against the parameter k, ranging from 0.02 to 0.035. The chaotic range $k_i \in [0.026, 0.03]$ is marked with red dotted lines. b) Time Evolution in Griffith's Chaotic Phase: Using a Global Coupled Map with $N = 10^3$ nodes, we plot states $X_t(i)$ over discrete time t. Initial transients of 10^5 steps are excluded. The phase is generated with coupling $\epsilon = 0.12$ and parameters $a = 0.89$, $b = 0.18$, $c = 0.28$. Each node has a randomly assigned k_i value in the range $k_i \in [0.026, 0.03]$.

Notions

- The plot clarifies the chaotic range under study. Specifically, our Chialvo Neuron Maps range includes some periodic windows.
- It is important noting the differences in the phases produced by Mechanism 2 compared to Mechanism 1. Specifically, Mechanism 2 emergence chaotic Griffith's Phase in Quadratic, Logarithmic, and Chialvo maps, while Mechanism 1 only does so in the Quadratic map.

3.1.3 Mechanism 3: Simultaneous Random Network and Parameter Heterogeneity.

To gain a comprehensive understanding, we combine Mechanism 1 and Mechanism 2 to investigate the effects of heterogeneity inside Erdös–Rényi network.

Main characteristics

The core attributes of this mechanism can be summarized as follows:

Table 3.3: Key Features of Mechanism 3

Feature	**Description**
Topology	Random. Erdös–Rényi topology.
Parameters in Local Dynamics	Heterogeneous. We have select the chaotic range of k.

Model

To incorporate Mechanism 1 into Coupled Map Networks, we use a system based on Erdős–Rényi topology, as outlined in Equation 3.1. Simultaneously we introduce parameter heterogeneity according ideas of 3.1.2. This approach aligns with the notion that learning involves making random connections before settling on a reliable path [learning quote]. This setup will help us determine whether the mechanism increases variability or extends the range of criticality.

Chialvo Neuron Map[82]

The Chialvo map captures excitable dynamics through the mentioned equations 3.5. We introduce heterogeneity in control parameter of local dynamics via Mechanism 2, distributing the perturbation-response parameter k_i uniformly and randomly across each node i within the range $k_i \in [0.026, 0.03]$.

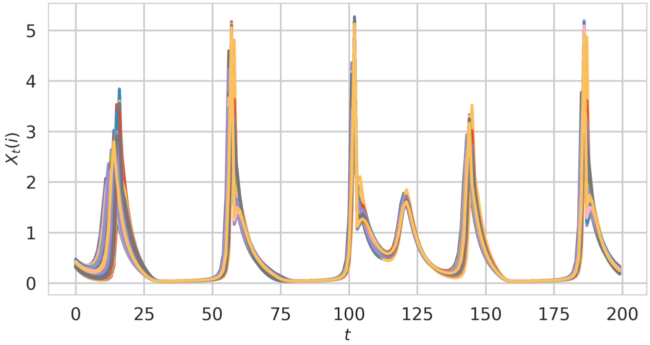

Figure 3.6: Temporal series of states $X_t(i)$ for an Erdös–Rényi network (Mechanism 1) with $N = 10^3$ nodes and an average of $k = 20$ neighbors. The discrete time variable t is used, and the first 10^5 transient steps are excluded. The phase is generated with a coupling constant $\epsilon = 0.21$ and parameters $a = 0.89$, $b = 0.18$, $c = 0.28$. For Mechanism 2, each node is assigned a k_i value, uniformly and randomly distributed in the range $[0.026, 0.03]$.

3.2 Measures behind criticality

In our exploration of the mechanism of emergence, we focus on three useful perspectives.

- **Probing Criticality**. First, we aim to confirm the critical behavior within certain ranges of the coupling constant ϵ, where the system spontaneously shows both synchronized and desynchronized states. The principal metric for validation is scale invariance, measured as a Power Law. We employ an auxiliary metric known as Maximum Cluster Evolution to get a consistent bin size.
- **State Characterization and Emergence**. The second perspective seeks to differentiate this unique state from other dynamical regimes. To achieve this, we introduce a novel measure, the "Dispersion of Fraction of Clusters," based on the definitions of synchronized and desynchronized clusters. This measure will help us to see the extent of Griffith's Chaotic Phase. Then, we will apply the Asymmetric Measure to provide a more detailed understanding of the phase's heterogeneity emergence.
- **Topology**. Finally, we will examine how topology influences the variability and extent of Griffiths Phase in Chialvo Neuron Maps using a Small World Network.

3.2.1 Power Law

> “Phenomena with the same beta exponent value belong in the same class. It's a fact that recalls the Platonic view of nature: it could be said that there are relatively few universality classes of critical behaviors, and each actual system leads back to one of these universality classes – in other words, in Plato's terms, to an Idea.”
> – *Giorgio Parisi, 2023, In a Flight of Starlings.*

A key indicator of a critical system is its scale-free nature. The term "scale-free" refers to a system that exhibits a power law, which describes a specific scaling relationship. In the context of avalanches, for example, a power law dictates that a certain ratio of cluster sizes will correspond to a specific ratio of cluster probabilities[35]. The property of scale invariance is evident in the uniform appearance of a straight line on a graph, indicating a consistent physics laws across different scales. However, it is important to note that this scale invariance eventually breaks down at extremely small or large scales. Therefore, the challenge in understanding complex systems lies in decoding the inherent power laws, particularly the exponents that define them[50]. For our study, this measure will proof the criticality behind each mechanism of emergence discussed in Section 3.1.

Mechanism 1: Random Topology

Let us review Kaneko's method to find the right bin size for Power Law analysis[6].

Quadratic Map

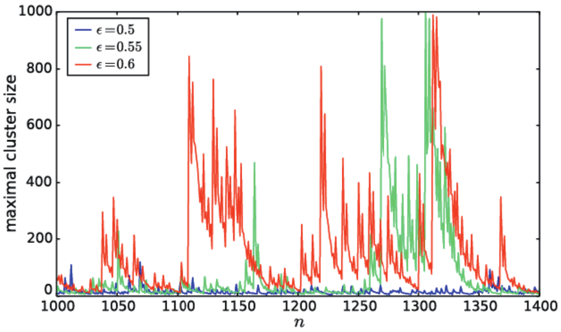

Figure 3.7: Temporal evolution of the maximal cluster size: $a = 1.7, k = 20$, and $N = 1000$. The cluster is computed by using the threshold $\delta = 10^{-3}$, while this intermittent behavior does not vary as long as it is sufficiently small. $\epsilon = 0.5$ (blue line), $\epsilon = 0.55$ (green line) $\epsilon = 0.6$ (red line), in the chaotic Griffiths phase[6].

Kunihiko Kaneko initially emphasized the temporal evolution of maximal cluster sizes to capture the recurring dynamics of synchronization and desynchronization. It is introduced a 'bin definition' δ for cluster measurement: Elements $x_t(i)$ that falls in same bin belong to a cluster, the number of elements inside this cluster will be the cluster size[6]. This methodology allows for the selection of an appropriate bin size that effectively captures the intermittent behavior of synchronization and desynchronization, thereby facilitating the quantification of Power Laws.

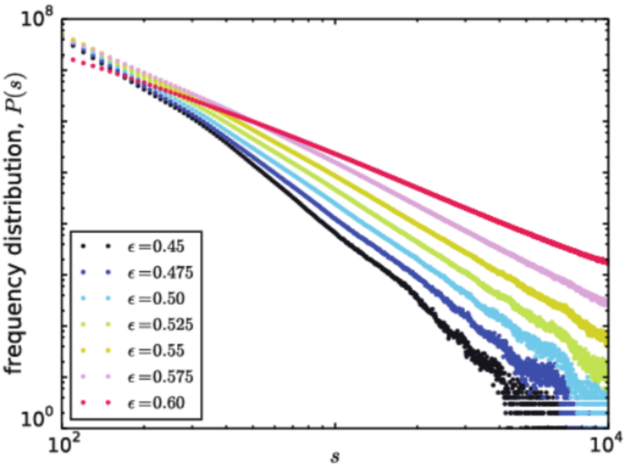

Figure 3.8: The distribution $P(s)$ of cluster size s. Log-log plot. $a = 1.7, k = 20$, and $N = 16384$. The results from $\epsilon = 0.45, 0.475, 0.5, 0.525, 0.55, 0.575$, and 0.6 are plotted with different colors. The distribution is obtained by sampling over 10^3 steps, with 100 initial conditions, over 100 networks, by using the threshold $\delta = 10^{-3}$, while the exponents do not vary as long as this threshold is sufficiently small, and also the network sample dependence is negligible. Figure is taken from[6].

As shown in Figure 3.8, a Power Law distribution emerges within a specific range of ϵ when Mechanism 1 is applied. Specifically, it is counted the frequency of clusters based on their size, revealing a Power Law phenomenon $P(s) \sim s^{-\alpha}$. Kunihiko Kaneko demonstrated that this exponent changes based on parameters a, ϵ, and k.

Notions

- Kunihiko Kaneko's method for counting clusters is not explicitly detailed, yet his work, useful results and emails interchanged offers valuable insights.

Mechanism 2: Heterogeneity in parameters

Several methods are available for counting clusters, including bin-based techniques with network creation strategies. We opt for the Matrix method, which is similar to methods used in network libraries but without network creation. This method is particularly efficient for systems with a large number of nodes N clearer in code A.0.1.

- **Initialization.** First, we consider our evolved States matrix, S_{matrix} with dimensions $(T + 1, N + 1)$. In this matrix, each row corresponds to a specific time instant t in the range $[0, T]$. Similarly, each column represents the state of an individual element from $X(0)$ to $X(N)$.

$$S_{matrix} = \begin{bmatrix} X_{t=0}(0) & \dots & X_{t=0}(N) \\ \vdots & \ddots & \vdots \\ X_{t=T}(0) & \dots & X_{t=T}(N) \end{bmatrix}$$

- **Distance Matrix.** We will select each one of the rows,

$$S_{\text{row}}[t, :] = [X_t(0), X_t(i), \dots, X_t(N)]$$

  and we will create a matrix of Distance between all nodes of each row. The new matrix D_t is the instant absolute difference between $S_{\text{row}}[t, :]$ and transpose of itself $S_{\text{row}}[t, :]^T$.

$$D_t[i,j] = \left|S_{\text{row}}[t,:] - S_{\text{row}}[t,:]^T\right| = \begin{pmatrix} 0 & |S_{\text{row}}[t,0] - S_{\text{row}}[t,1]| & |S_{\text{row}}[t,0] - S_{\text{row}}[t,2]| & \cdots \\ |S_{\text{row}}[t,1] - S_{\text{row}}[t,0]| & 0 & |S_{\text{row}}[t,1] - S_{\text{row}}[t,2]| & \cdots \\ |S_{\text{row}}[t,2] - S_{\text{row}}[t,0]| & |S_{\text{row}}[t,2] - S_{\text{row}}[t,1]| & 0 & \cdots \\ \vdots & \vdots & \vdots & \ddots \end{pmatrix}$$

- **Extracting Connections.** We extracts the first diagonal above the main diagonal from D_t into an array connections.

  $$\text{C[k]} = \text{connections} = \text{First Upper Diagonal} = [D[0,1], D[1,2], \ldots, D[N-1,N]]$$

  Where C[k] is the connection element between i and j.

- **Clustering Function.** This function takes a list of connections and a threshold δ to identify clusters.

  $$\text{Count}_{\text{cluster}} \leftarrow \begin{cases} \text{Count}_{\text{cluster}} + 1 & \text{if } C[k] \leq \delta \\ 0 & \text{if } C[k] > \delta \\ \text{Count}_{\text{cluster}} & \text{otherwise} \end{cases}$$

  Finally, it returns sizes and frequency of each cluster.

Quadratic Map.

Equations followed in 3.1.2.

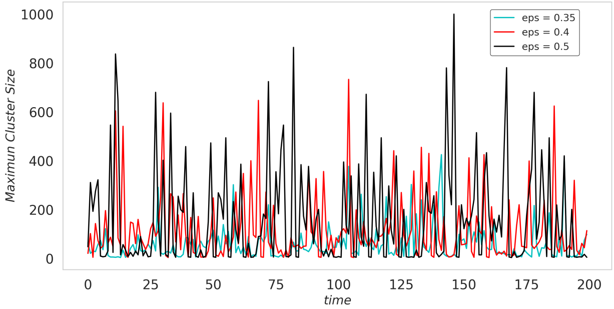

Figure 3.9: Time Series of Maximum Cluster Size: The data is generated from a Global Coupled Network with $N = 1000$ nodes, each assigned a parameter a_i in the range $[1.6, 2.0]$. The bin size used for the plot is $\delta = 10^{-4}$. Different colored lines represent varying coupling strengths: $\epsilon = 0.35$, $\epsilon = 0.4$, and $\epsilon = 0.5$, all of which fall within the chaotic Griffith's Phase.

Figure 3.9 shows the evolution of the largest cluster size in our quadratic coupled equations. This visualization guided us to choose a bin size of $\delta = 10^{-4}$ for obtaining the Power Law using code A.0.1.

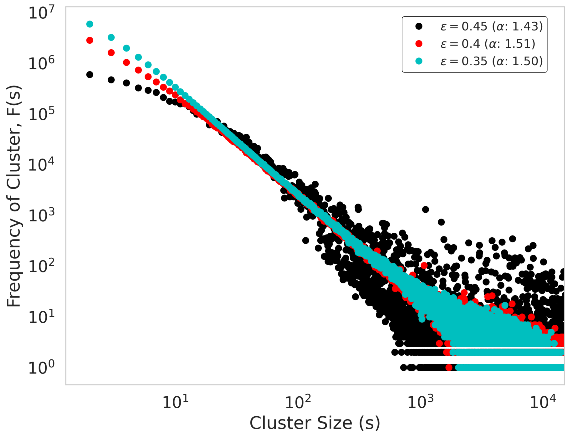

Figure 3.10: **Power Law Distribution**: In this log-log plot, we examine cluster size distribution ($F(s)$) within a globally coupled network of $N = 16,000$ nodes which operate with heterogeneity $a_i \in [0.026, 0.03]$. Three coupling strengths ($\epsilon = 0.35, 0.4$, and 0.45) are represented by distinct colors. Data is from 20 networks observed over 10^3 steps, using a cluster-counting bin size of $\delta = 10^{-4}$. Exponents α are calculated with Python's `powerlaw` library, sensitive to ϵ.

As evident from Figure 3.10, the observed behavior follows to a Power Law, $P(s) \sim s^{-\alpha}$.

Notions

- As ϵ increases, the tail of the distribution begins to spread, influenced the choice of an appropriate bin. Our selection is guided by the behavior of the Maximum Cluster Evolution, although the methodology for bin selection is not universal depends on your dynamical system.

Chialvo Maps

Equations described in Subsection 3.1.2.

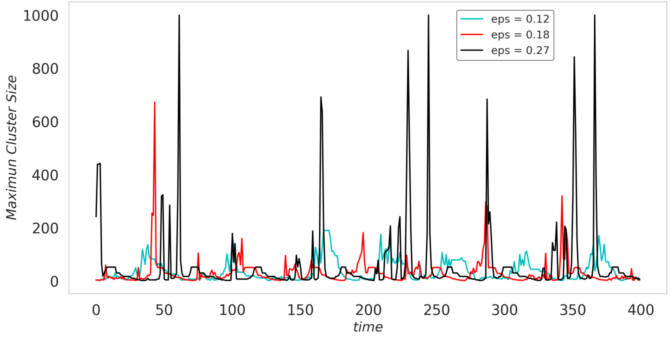

Figure 3.11: **Time Series of Maximum Cluster Size.** The data is generated from Globally Coupled Network of $N = 1000$ nodes, each assigned a parameter $k_i \in [0.026, 0.03]$. The bin size used for the plot is $\delta = 10^{-5}$. Different colored lines represent varying coupling strengths: $\epsilon = 0.12$, $\epsilon = 0.18$, and $\epsilon = 0.27$, all within the chaotic Griffith's Phase.

The graph in Figure 3.11 illustrates the evolution of the largest cluster size, guiding our choice of a bin size $\delta = 10^{-5}$ for calculating the Power Law, using code A.0.1.

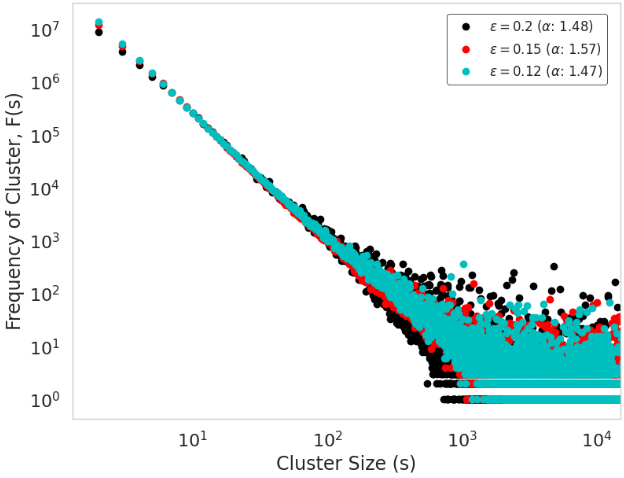

Figure 3.12: Power Law Distribution. We analyze the distribution $F(s)$ of cluster sizes s using a log-log plot. Data comes from a globally coupled Chialvo Neuron Maps with $N = 16000$ nodes. Each node with $k_i \in [0.026, 0.03]$ uniformly and randomly assigned. We present results for three different coupling strengths—$\epsilon = 0.12, 0.15$, and 0.2—each distinguished by color. The data is aggregated from 20 unique networks and observed over 10^3 steps. We use a bin size of $\delta = 10^{-5}$ for cluster counting. The exponent α, is calculated using Python's `powerlaw` library.

As illustrated in Figure 3.12, the time series behavior of Chialvo Coupled Maps from Figure 3.5 aligns with a Power Law, $P(s) \sim s^{-\alpha}$. This highlights the need for an optimal bin size, guided by the Maximum Cluster Evolution, and confirms criticality within a specific ϵ range. Notably, the exponent α changes with increasing ϵ.

Notions

- The choice of bin size is often non-trivial in the analysis of power laws. Despite the time series illustrated in Figure 3.3, we did not find any signs of a power law from Global Coupled logarithmic maps with varying parameter b_i. This suggests some possibilities: First, we are not inside a Griffiths Phase, as there is no critical behavior. It could represent a different type of phase transition with a unique distribution or it can be a special case of robust chaos Griffiths Phase requiring a unique bin size.

Mechanism 3: Simultaneous Random Network and Heterogeneity in Parameters.

Chialvo Maps

To confirm the criticality emergence from this dual mechanism presented in subsection 3.1.2, we opt for Counting method of clusters A.0.1, particularly effective for handling large N.

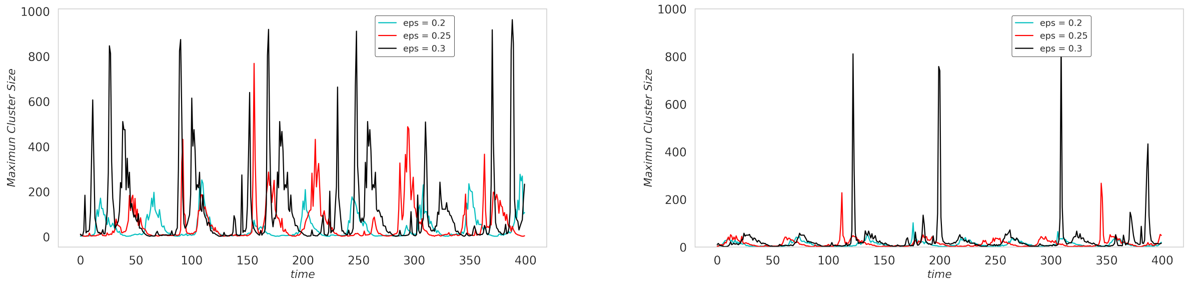

Figure 3.13: a) Time Series of Maximum Cluster Size. The data is obtained from an Erdös–Rényi network consisting of 1000 nodes with an average of K=20 neighbors. Each node is assigned a parameter k_i that follows a uniform random distribution in the range of [0.026 to 0.03]. The bin size for the plot is set to $\delta = 20^{-5}$. The different colored lines on the graph represent various coupling strengths ϵ: 0.2, 0.25, and 0.3. All of these values fall inside the chaotic Griffith's Phase. b) Similar to (a), but with a bin size of $\delta = 10^{-5}$.

The Figure 3.35 shows the evolution of the largest cluster size, capturing intermittent behavior between synchronization and desynchronization. Two bin sizes, $\delta = 2 \times 10^{-5}$ and $\delta = 10^{-5}$, were considered. Based on these observations, we chose a bin size of $\delta = 10^{-5}$ for calculating the Power Law, as detailed in code A.0.1.

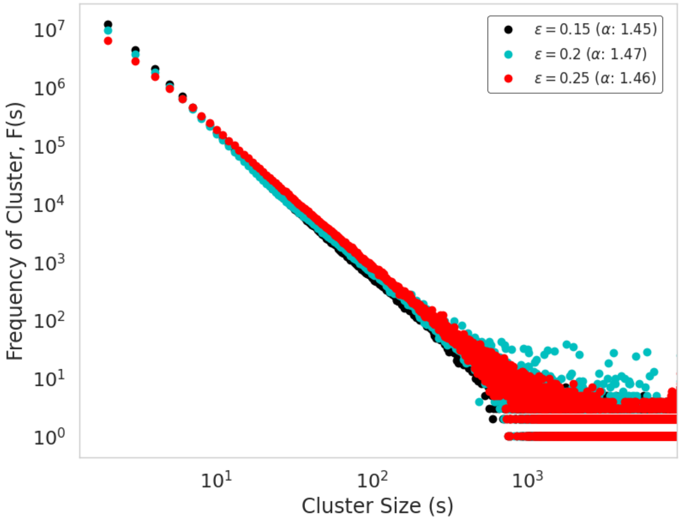

Figure 3.14: Power Law Distribution. In the Log-Log plot, we examine the distribution $F(s)$ of cluster sizes s in a Erdös–Rényi network of $N = 10000$ nodes. Each node operates with the Chialvo Neuron Map, with k_i parameters uniformly distributed im range [0.026, 0.03]. We present results for three different coupling strengths—$\epsilon = 0.15, 0.2$, and 0.25—each distinguished by color. The data is compiled from 20 unique networks, each observed over 10^3 steps. We employ a cluster-counting bin size of $\delta = 10^{-5}$. The exponent α is computed using Python's `powerlaw` library.

As shown in Figure 3.14, the data follows a Power Law distribution $P(s) \sim s^{-\alpha}$, confirming criticality within a specific range of ϵ. This is in line with the time series behavior observed for Chialvo Coupled Maps in an Erdös–Rényi network, as seen in Figure 3.6. Importantly, the exponent α varies with changes in ϵ.

3.2.2 Dispersion of Fraction of Clusters (DFC)

"States inside chaotic Griffiths phase seems to evolve as ill-formed clusters" — Mario Cosenza

To understand the extent of the chaotic Griffith's Phase and differentiate it, we focus on the time series behavior where elements synchronize and desynchronize spontaneously. This concept of travel between states lead us to develop a new measure called Dispersion Fraction of Cluster. Specifically, we join two established measures for this purpose: One for cluster detection and another for identifying dispersion within those clusters.

Measure 1: Fraction of Clustered Elements. For this measure, elements i and j are considered part of a cluster at time t if their state variables are within a distance δ. States difference are defined as $d_{ij}(t) = |x_t^i - x_t^j|$. The threshold δ depends on the dynamical system. The fraction of clustered elements at time t is then calculated as in[89]:

$$p(t) = 1 - \frac{1}{N}\sum_{i=1}^{N}\prod_{j=1,j\neq i}^{N}\Theta(d_{ij}(t)-\delta),$$

where $\Theta(x)$ is the Heaviside step function.

$$\Theta(x) = \begin{cases} 0 & \text{if } x < 0, \\ 1 & \text{if } x \geq 0. \end{cases}$$

Once we measure fraction of elements that belong to some cluster, we can apply the second measure.
To elucidate the functionality of this measure, consider a Globally Coupled Chialvo Neuron Map with parameters heterogeneity, analyzed in Equations 3.5. This system manifests three distinct phases: Synchronization, Desynchronization, and chaotic Griffiths Phase. We examine the fraction of elements that belongs to a cluster:

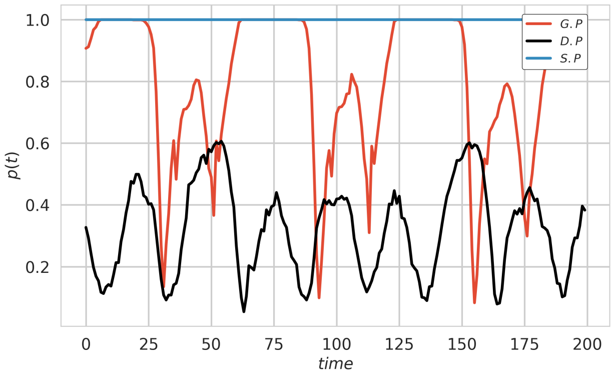

Figure 3.15: Fraction of Clusters: The plot displays the variable p_t calculated over different time series corresponding to $\epsilon = 0.05$ (black line), 0.13 (red line), and 0.55 (blue line). These values of ϵ represent varying degrees of interaction in a Globally Coupled Chialvo Neuron Map system with $N = 1000$. Parameters are set as $a = 0.89$, $b = 0.18$, $c = 0.28$, and k ranges from 0.026 to 0.03. Labels on the plot indicate collective states: D.P for Desynchronization Phase, G.P for chaotic Griffith's Phase, and S.P for Synchronization Phase.

The figure reveals the extensive dispersion range exhibited by time series inside the Griffith's Phase (red-line). In this region $p(t)$ uniquely travels from high synchronization to pronounced desynchronization. Subsequently, we introduce a second metric to quantify this high variability.

Measure 2: Dispersion of Fraction of Clusters. To differentiate between synchronized, desynchronized and critical states, we compute the time-averaged standard deviation σ. The standard deviation applied to the fraction of clusters $\sigma(p_t)$ is given by

$$\sigma(p_t) = \sqrt{\frac{1}{N}\sum_{i=1}^{N}\left(p_t^i - \bar{p}_t\right)^2},$$

where $\bar{p}_t$ is the average state at time t, defined as

$$\bar{p}_t = \frac{1}{N}\sum_{j=1}^{N} p_t^j.$$

The quantity $\sigma(p_t)$, **Dispersion of Fraction of Clusters (DFC)**, quantifies the spontanious variability in the states of clusters. It illustrates the extent of the critical region in the interaction parameter defined by ϵ, facilitating its differentiation from other dynamical phases.

Mechanism 1: Random Topology

Quadratic Map

Let us examine DFC metric within the range of the Griffith's Phase to discern the extension of this critical region, and verify its consistency with Shinoda and Kaneko phase space[6].

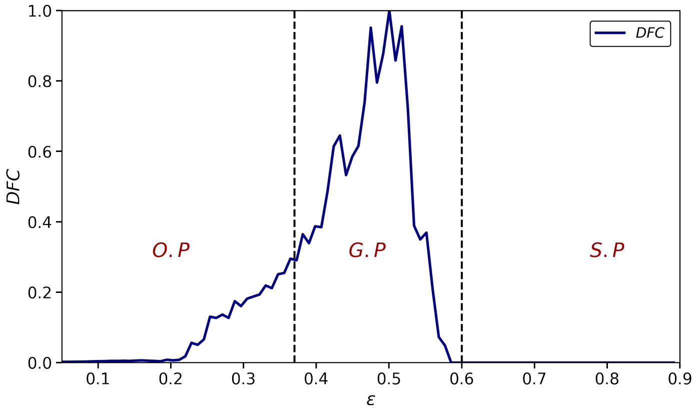

Figure 3.16: Dispersion of Fraction of Clusters (*DFC*). Plotted as a function of the coupling constant ϵ over the range [0.05, 0.9], divided into 100 uniform steps. A bin size of 10^{-3} is used in the *DFC* for cluster identification. Calculations are performed for a Erdös–Rényi network of $N = 100$ nodes with $a = 1.7$ and $K = 20$. Averages for *DFC* are taken over 20 realizations, each with 10^5 transients discarded and uniformly random initial conditions in range [0, 1]. Labels indicate collective states: G.P for Griffith's Phase, S.P for Synchronization Phase and O.P for Other Phases. Dotted black lines represent limits according the time series.

In our *DFC* analysis presented in Figure 3.16, we focus on systems with a Low number of nodes N. We consider this advantage as a feature of scale-invariant demonstrated in Figure 3.8.

Notions

- Our measure picks align well with K. Shinoda and K. Kaneko Phase Space, but slight adjustments in the lengths may be needed for the counting of other potential near phases such as the Order Phase or Chimera Phase.

Mechanism 2: Heterogeneity in parameters

Quadratic Map

The primary role of DFC is to assess the extent of the Griffiths Phase in quadratic maps generated by Mechanism 2 discussed in Section 3.1.2, which does not involve random topology. The equations used are described in Section 3.1.2.

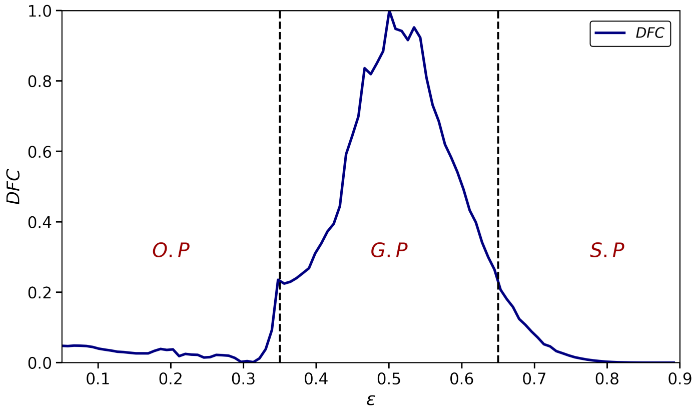

Figure 3.17: Dispersion of Fraction of Clusters (DFC): The plot shows the normalized *DFC* as a function of the coupling constant ϵ, ranging from 0.05 to 0.9. This is based on a Global Coupled network of $N = 100$ nodes, each node with a parameter $a_i \in [1.6, 2.0]$. *DFC* is averaged over 20 runs, disregarding the first 10^5 steps in each run. A bin size of 10^{-3} is used in the *DFC* for cluster identification. Initial node conditions are uniformly distributed between 0 and 1. Labels such as *O.P*, *G.P*, and *S.P* indicate Other Phases, Griffith's Phase, and Synchronization Phase, respectively. Dotted black lines mark time-series-based limits.

Notably, the extent of the Griffiths Phase slightly increases. To better understand this phase transition, we will examine the time series just before and after the Griffiths Phase. As Kaneko suggests, the Chaotic Griffiths Phase is typically detected when global synchronization is lost.

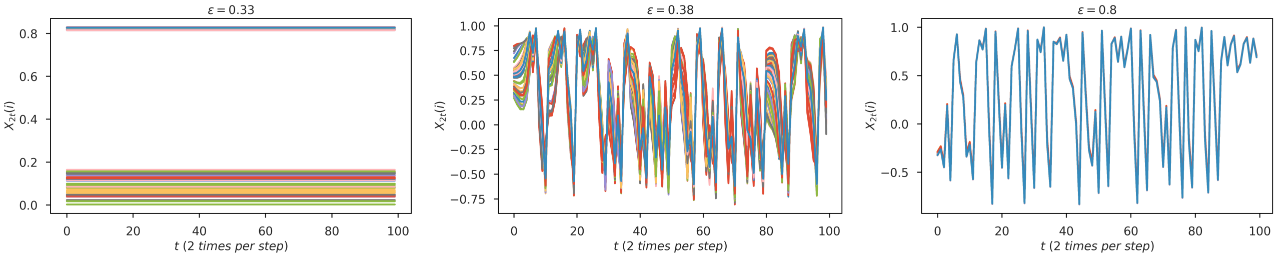

Figure 3.18: Time series of Global Coupled Quadratic Map. Order Phase at $\epsilon = 0.33$, Synchronization Phase at $\epsilon = 0.8$, and, at the peak of DFC with $\epsilon = 0.38$ belonging to the Griffith's Phase. All observations are made with $N = 100$ nodes, employing correspondence mechanism 2, detailed in 3.1.2.

The time series helps to explain the presence or absence of peaks in our measure plotted in Figure 3.17. Specifically, three distinct phases can be identified:

- **Other Phases (O.P)** : Before the first dotted line, which marks the beginning of a high DFC peak, we see both a Desynchronized Phase and an Ordered Phase. Last is showed in Figure 3.18 with a coupling constant $\epsilon = 0.33$.

- **Chaotic Griffiths Phase (G.P)**: The interval where the DFC measure increases corresponds to the chaotic Griffiths Phase, supported by the time series in Figure 3.18 at $\epsilon = 0.38$.
- **Synchronized Phase (S.P)**: After the second dotted line, which marks the end of the high DFC peak region, a Synchronized Phase is observed, as shown in Figure 3.18 at $\epsilon = 0.8$.

Notions

- The presence of low peaks outside the Griffiths Phase is minimal and could be attributed to two factors: First, these peaks may indicate the existence of other detectable states, such as Chimera States or Chaotic Itinerancy. Second, the choice of bin size, which is specific to each dynamical system, could also contribute to these low peaks. Importantly, neither of these factors compromises the clear identification of the Griffiths Phase.

Logarithmic Map

It is worth noting that our measure effectively captures the extent of regions that exhibitis intermittent behavior between synchronization and desynchronization. Particularly, we present the case of Global Coupled Logarithmic Maps with heterogeneity in parameter $b_i \in [-1, 1]$ specified in equations 3.4:

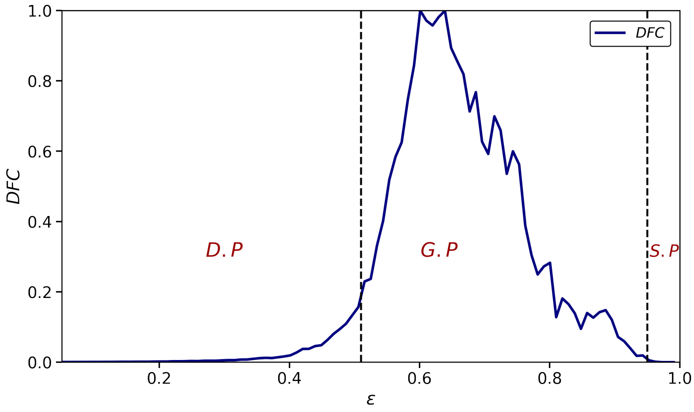

Figure 3.19: Dispersion of Fraction of Clusters (DFC): The normalized DFC is plotted as a function of the coupling constant ϵ, which varies from 0.05 to 1. Counted states comes from Global Coupled Logarithmic Maps with $N = 100$ nodes, each assigned a randomly parameter $b_i \in [-1, 1]$. The DFC values are averaged over 20 networks, each discarding the first 10^5 transient steps and using uniformly random initial conditions in the range $[0, 1]$. A bin size of 10^{-3} is employed for counting clusters. We note each phase, D.P, "G.P", and S.P represent Desynchronization, "Griffiths", and Synchronization Phases.

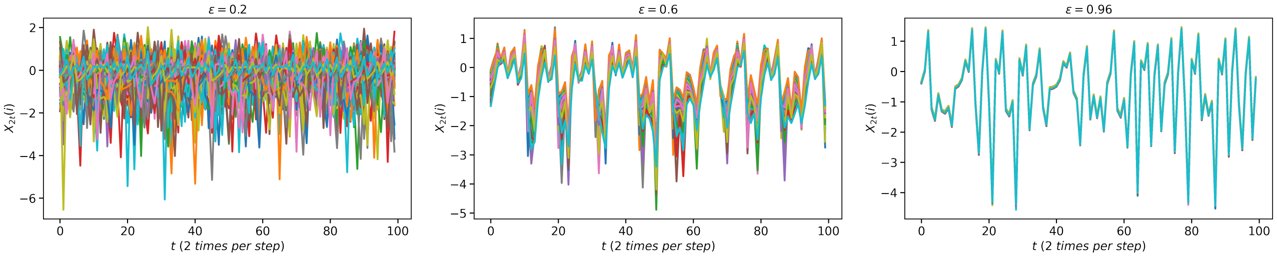

Figure 3.20: Time series for Global Coupled Logarithmic Maps reveal distinct phases: Desynchronization Phase at $\epsilon = 0.2$, "Griffiths Phase" at $\epsilon = 0.6$, and Synchronization Phase at $\epsilon = 0.96$. Data is from a $N = 100$-node network governed by mechanism 2, detailed in Section 3.1.2

Clearly, time series help us to distinguish the scaling range of DFC behind Logarithmic Map in Figure 3.19.

Notions

- To follow the phenomena. Label 'G.P' means a possible Griffiths Phase. Even more, this phenomenon is not precisely a Griffiths Phase, as it does not exhibit a Power Law, as mentioned in Notions 3.2.1.

Chialvo Neuron Map

The significance of the critical region within Global Coupled Chialvo Neuron Maps is discussed in Section [BrainCriticality]. In specific, we examine the Chialvo Map's criticality using heterogeneity with $k_i = [0.026, 0.027]$ parameter range. The DFC metric is designed to illustrates the extent of the chaotic Griffiths Phase and impact of heterogeneity on criticality, which emerges from Mechanism 2 presentend in Figure 3.5 and confirmed by the Power Law in Figure 3.12. The equations used are specified in Section 3.1.2.

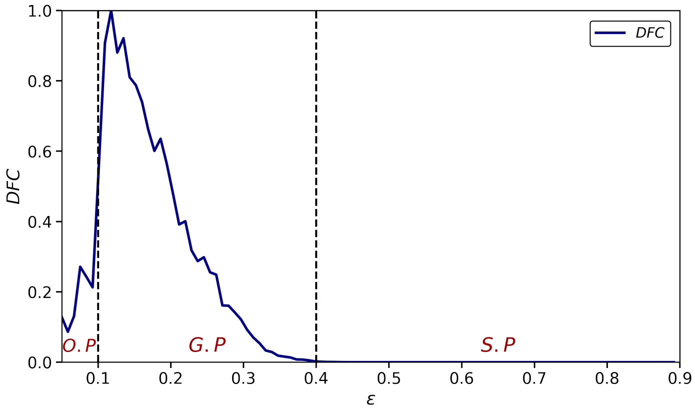

Figure 3.21: Dispersion of Fraction of Clusters (DFC): The normalized DFC is plotted as a function of ϵ, ranging from 0.05 to 0.9. The data is derived from Global Coupled Maps with $N = 100$ nodes, each assigned a randomly parameter uniformly distributed in the range $k_i \in [0.026, 0.03]$. DFC is averaged over 20 runs, omitting the first 10^5 steps with different initial conditions [0,1]. A bin size of 10^{-3} is used for DFC. Labels O.P, G.P, and S.P signify Other, Griffiths, and Synchronization Phases, respectively.

To elucidate the underlying phases associated with DFC peaks presented in Figure 3.21, we will analyze the time series before, during, and after the dotted black lines.

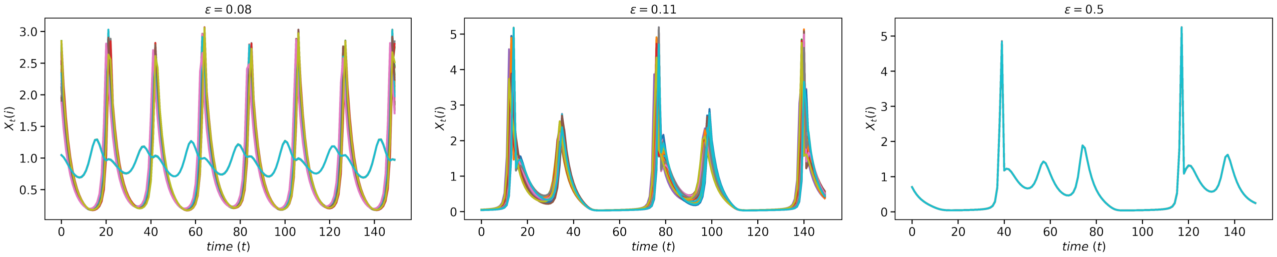

Figure 3.22: Time series for Global Coupled Chialvo Maps are presented for three distinct phases: The Chimera Phase at $\epsilon = 0.08$, the Synchronization Phase at $\epsilon = 0.5$, and the Griffith's Phase at the DFC peak with $\epsilon = 0.11$. All data are collected from a network of $N = 100$ nodes, in accordance with mechanism 2, as developed in Section 3.1.2.

The time series in Figure 3.22 identifies three key phases related with the peak in our DFC measure showed in Figure 3.21:

- **Other Phases (O.P):** Previous to the first dotted line, which signifies the onset of DFC peak, we observe both Desynchronized and Chimera Phases. Chimera is illustrated in Figure 3.22 with a coupling constant $\epsilon = 0.08$.
- **Chaotic Griffiths Phase (G.P):** The region where the DFC measure rises corresponds to the Chaotic Griffiths Phase, corroborated by the time series in Figure 3.22 at $\epsilon = 0.11$.
- **Synchronized Phase (S.P):** Posterior the second dotted line, marking the end of DFC peak, a Synchronized Phase is evident, as depicted in Figure 3.22 with $\epsilon = 0.5$.

To improve the understanding between heterogeneity and the extent of criticality, we will recalculate our DFC measure using the Chialvo Map Equations. This time, however, we will use a narrower range of heterogeneity, specifically $k_i \in [0.026, 0.027]$.

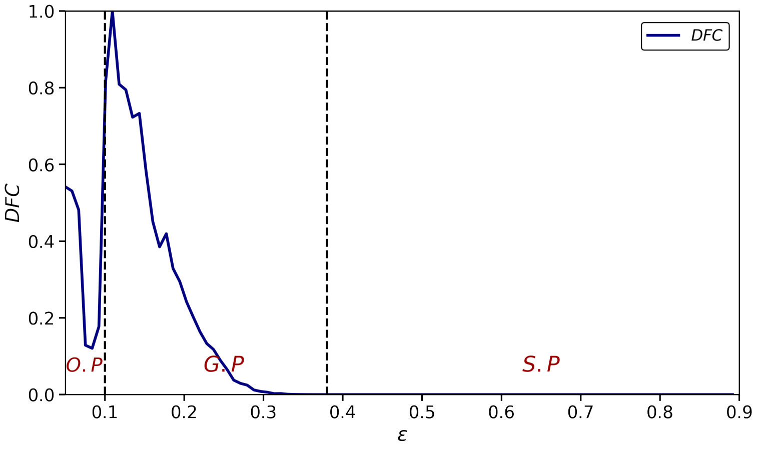

Figure 3.23: Dispersion of Fraction of Clusters: The plot illustrates the metric DFC in blue as a function of ϵ, spanning from 0.05 to 0.9. Calculations are based on a Global Coupled Maps of $N = 100$ nodes, each with a local parameter k_i in the range $[0.026, 0.027]$. DFC is averaged over 20 runs with initial conditions taken in range [0,1], and omitting the first 10^5 steps. A bin size of 10^{-3} is used for measure DFC. Labels O.P, G.P, and S.P signify Other Phases, Griffiths Phase, and Synchronization Phase.

Notions

- The key difference between Figure 3.23 and Figure 3.21 lies in the range of heterogeneity examined. When k_i is confined to $[0.026, 0.027]$, criticality narrows slightly. On the other hand, a k_i range of $[0.026, 0.03]$ broadens the critical region. These ranges are chosen to maintain consistent neuronal behavior. Yet, if we avoid this constraint and opt for a wider k_i range of $[0.026, 0.06]$, synchronization phase dissapears. This phenomenon of extend criticality with heterogeneity has been previously documented[83].

Chialvo Neuronal Map with spatial and Topological Heterogeneity

The Dispersion of Fraction of Clusters measure in mechanism 3 is crucial as it expose how simultaneous random topology and heterogeneity affect the Griffiths Phase compared with mechanism 2 (only heterogeneity in parameters) in terms of the extent and shape of DFC. For this analysis, we use the Chialvo Maps equations, given by Equation 3.5, along the topology defined in mechanism 1, Equation 3.1.

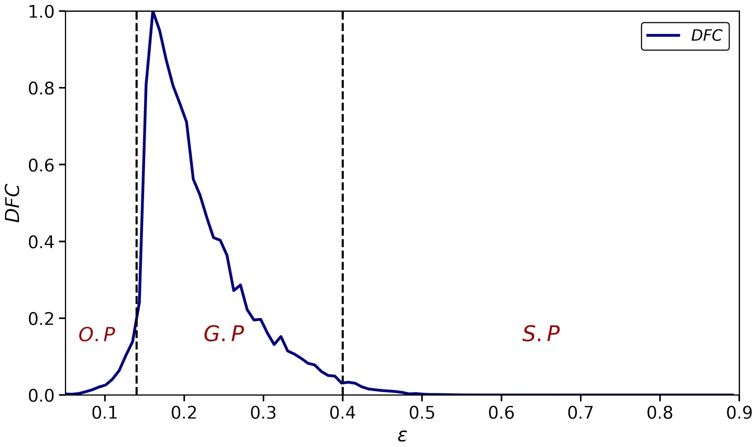

Figure 3.24: The plot displays the Dispersion of Fraction of Clusters (DFC), illustrated in blue, as a function of ϵ which ranges from 0.05 to 0.9. The calculations are performed on an Erdös–Rényi Network with $N = 100$ nodes and an average of $K = 20$ neighbors per node. Each node has a local parameter k_i within the range $[0.026, 0.03]$. The DFC values are averaged over 20 runs, disregarding the initial 10^5 steps. A bin size of 10^{-3} is employed for DFC. The labels signify O.P: Other Phases, G.P: Griffiths Phase, and S.P: Synchronization Phase.

Let's examine the time series at three key points: before, during, and after the peak of DFC shown in Figure 3.24.

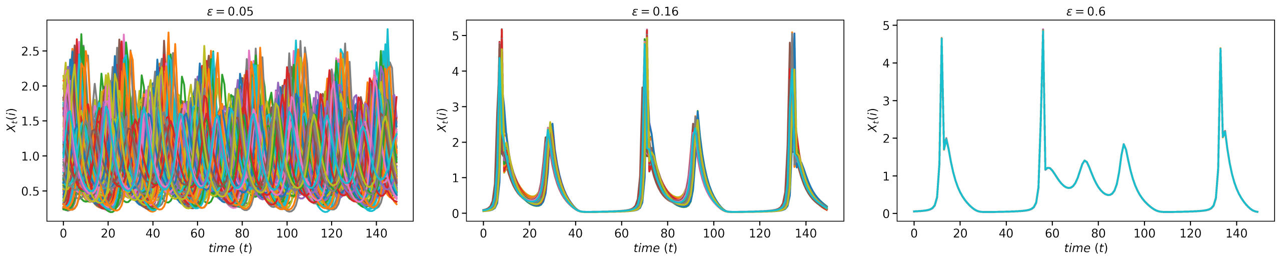

Figure 3.25: The time series describes a notable peak in our measure, marking three distinct phases: the Desynchronization at $\epsilon = 0.05$, the Synchronization Phase at $\epsilon = 0.16$, and the Griffith's Phase at the peak of DFC with $\epsilon = 0.6$. All data are collected from a network of $N = 100$ nodes using correspondence mechanism 2.

Time series in Figure 3.25 highlights three main phases that explains DFC from Figure 3.24:

- **Desynchronization Phase (D.P):** Located before the first dotted line marking the start of the DFC peak, we see Desynchronized Phase with a coupling constant $\epsilon = 0.05$.
- **Chaotic Griffiths Phase (G.P):** The DFC peak aligns with the Chaotic Griffiths Phase, confirmed by the time series at $\epsilon = 0.16$
- **Synchronized Phase (S.P):** After the second dotted line, which marks the end of DFC peak, a Synchronized Phase is clearly visible at $\epsilon = 0.6$

To ensure an extended range of criticality using mechanism 3, we investigate the critical behavior of the Chialvo Map within the parameter range $k_i = [0.026, 0.027]$.

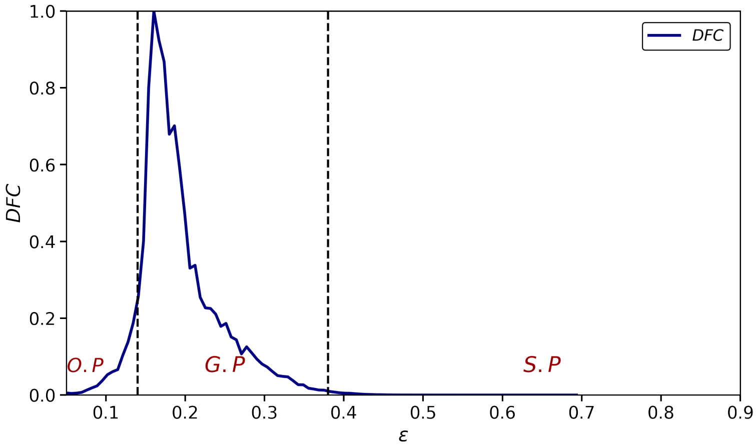

Figure 3.26: Dispersion of Fraction of Clusters (DFC) in blue, as a function of ϵ that varies from 0.05 to 0.9. The analysis is based on an Erdös–Rényi Network with $N = 100$ nodes and an average of $K = 20$ neighbors per node. Each node has a local parameter k_i in the range $[0.026, 0.027]$. DFC values are averaged over 20 runs, omitting the initial 10^5 steps. A bin size of 10^{-3} is used for DFC. Labels such as O.P., G.P., and S.P. stand for Other Phases, Griffiths Phase, and Synchronization Phase, respectively.

As we can see in Figure 3.26 compared with result in Figure 3.24, the extend of criticality has a relation with heterogeneity. This is consistent with Notion 3.2.2.

3.2.3 Asymmetry Measure

To understand the relation between emergence of chaotic Griffiths Phase and heterogeneity. We introduce an asymmetry measure[90]. This is a control parameter A that varies between 0 and 1 to evaluate the system heterogeneity. The individual parameters r_i are computed as

$$r_i = R_1 + A\xi(R_2 - R_1), \tag{3.6}$$

where ξ is a uniformly distributed random number between 0 and 1. For $A = 0$, all r_i values become identical, leading to a homogeneous system. On the other hand, for $A = 1$, r_i considers the full range $[R_1, R_2]$, maximizing system heterogeneity. As it turns out, A sets the range for r_i as

$$r_i \in [R_1, R_1 + A(R_2 - R_1)] \tag{3.7}$$

We will calculate our metric, DFC, in terms of this Asymmetry Measure A. The parameter A relates the level of heterogeneity in the system and emergence of chaotic Griffiths Phase.

Mechanism 2

Quadratic Map

The equations for DFC are outlined in Section 3.2.2, while the equations detailing quadratic heterogeneity can be found in Equations 3.3.

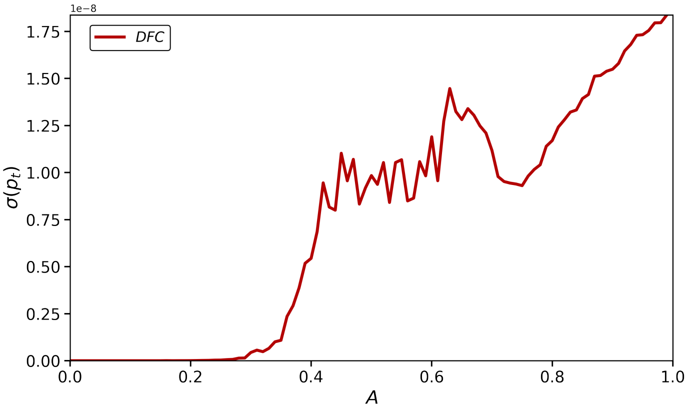

Figure 3.27: The Dispersion of Fraction of Clusters (DFC) is plotted against the asymmetry parameter A for globally coupled quadratic maps consisting of $N = 100$ nodes with heterogeneity $a_i \in [1.6, 2.0]$, as specified in Equations 3.3. The coupling constant is set at $\epsilon = 0.41$. This plot is generated from 20 realizations.

Notions

- Interestingly, the evolution of the asymmetry parameter presented in figure 3.27 is constant, but it is not linear. It exhibits peaks at partial heterogeneity values of 0.4 and 0.7 within DFC measure. This is observed with a fixed $\epsilon = 0.41$, which lies within the Griffiths Phase region.

Logarithmic Map

The equations governing DFC are outlined in Section 3.2.2, while the equations specific to logarithmic heterogeneity can be found in Equations 3.4.

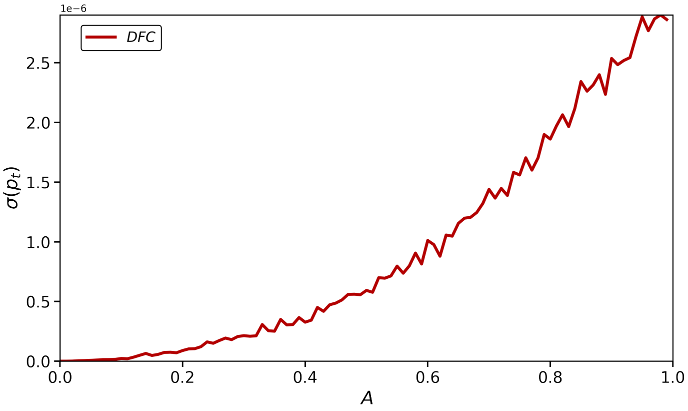

Figure 3.28: The plot displays the Dispersion of Fraction of Clusters (DFC) as a function of the asymmetry parameter A. It is based on globally coupled Logarithmic maps with $N = 100$ nodes and each node heterogeneity $b_i \in [0, 1]$, as outlined in Equations 3.4. The coupling constant is set at $\epsilon = 0.61$, and the data is derived from 20 different realizations.

Figure 3.28 presents the constant growth evolution of DFC in terms of asymmetry parameter. This is observed with a fixed $\epsilon = 0.61$, which lies within the "Griffiths Phase" region (see Notion 3.2.1).

Chialvo Neuronal Map

We focus solely on mechanism 2. The equations for DFC are described in Section 3.2.2, and the equations related to Chialvo Neuron Maps with heterogeneity are detailed in Equations 3.5.

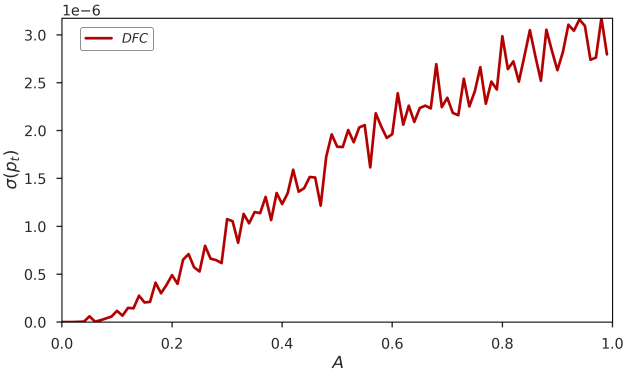

Figure 3.29: The plot shows the Dispersion of Fraction of Clusters (DFC) against the asymmetry parameter A. It uses globally coupled Chialvo maps with $N = 100$ nodes, each having a heterogeneity parameter k_i in the range $[0.026, 0.03]$, as specified in equations 3.5. The coupling constant is fixed at $\epsilon = 0.12$, and the plot includes data from 20 different realizations.

Figure 3.29 shows the steady increase of DFC as a function of the asymmetry parameter A. This behavior is observed with a constant coupling value of $\epsilon = 0.12$, which falls within the critical region.

Mechanism 3

Chialvo Neuronal Map

We focus on mechanism 3. The equations governing DFC are outlined in Section 3.2.2. The equations representing neuron behavior, specifically using Chialvo Neuron Maps with heterogeneity, are detailed in Equations 3.5. These equations are sampling over a Erdös–Rényi Network taken from Equation 3.1.

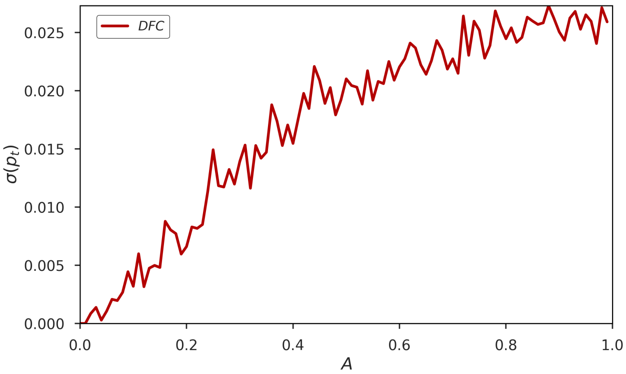

Figure 3.30: Dispersion of Fraction of Clusters (DFC) as a function of the asymmetry parameter A. It is based on Chialvo Networks coupled through an Erdös–Rényi topology with $N = 100$ nodes and an average of $K = 20$ neighbors per node. Each node has a heterogeneity parameter k_i in the range [0.026, 0.03], as described in Equations 3.5. The coupling constant is set at $\epsilon = 0.17$, and the data is derived from 20 different realizations.

Notions

- Figure 3.30 illustrates the consistent rise of DFC in relation to the asymmetry parameter A. This trend is observed with a fixed coupling value of $\epsilon = 0.17$, which lies within the Griffiths Phase. Notably, the magnitude of DFC is higher in this figure compared to Figure 3.29. Additionally, the emergence of the Griffiths Phase, indicated by peaks in DFC, occurs with slightly less heterogeneity compared to Figure 3.29.

3.2.4 Small World Network

We explore the topology of our network in greater detail by examining its Small World characteristics, introducing a new rewiring parameter p for this analysis. Generally, the topology influenced by this parameter is more easily understood through the following illustration[7]:

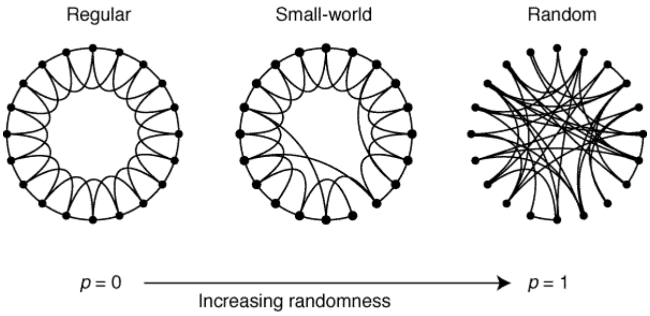

Figure 3.31: The figure depicts the rewiring process guided by parameter p in a Network. At $p = 0$, the network is regular; at $p = 1$, it becomes random. Intermediate values of p represents an Small World Network. Illustration taken from[7].

Main characteristics

The core attributes used to produce Griffiths Phase in this section can be visualized as follows:

Using Small World network we employ in local dynamics the Chialvo Neuron Maps with mechanism 2, focusing on parameter heterogeneity k_i, see Equations 3.5. Fixing parameter interaction parameter *epsilon*, this sets expectations of distinct dynamics in rewiring parameter boundaries. At $p = 0$, the regular network should deviates from critical dynamics

Table 3.4: Key Features of Small World Network with Chialvo Maps

Feature	**Description**
Topology	Small World Network
Parameters in Local Dynamics	Heterogeneous. We have select the chaotic range of k.

due to limited degrees of freedom. At $p = 1$, high system variability leads to Griffiths Phase dynamics. Our aim is to explore temporal series of the Griffiths Phase within the Small World Network range, situated between these extremes.

Proof of Small World Network

Specifically, we consider a network of N=100, K=40 and p=0.038. We need to proof that our network falls into Small World Network highlighting two key features[7]:

- *High clustering* C_p/C_0
- *Short path length* L_p/L_0

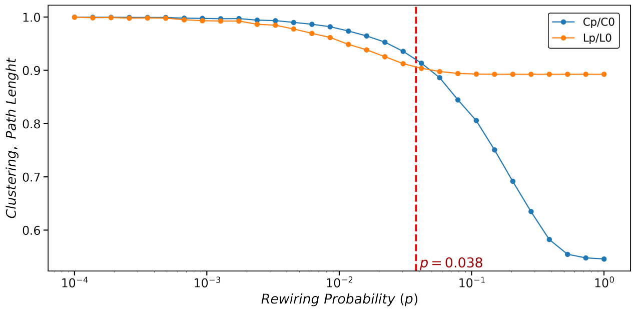

Figure 3.32: Clustering (in blue) and Path Length (in orange) are plotted as functions of the parameter p. X-axis is in log-scale. N=100, K=40 averaged over 30 samples, a red dotted line marks the network configuration we will use, with a rewiring parameter set at $p = 0.038$.

Dispersion of the Fraction of Clusters (DFC)

Using $p = 0.038$ we employ Chialvo Neuron Maps as local dynamics the inside our Small World Network. Focusing on parameter heterogeneity k_i, see Equations 3.5. To get clearly our emerged phases, let us calculate DFC.

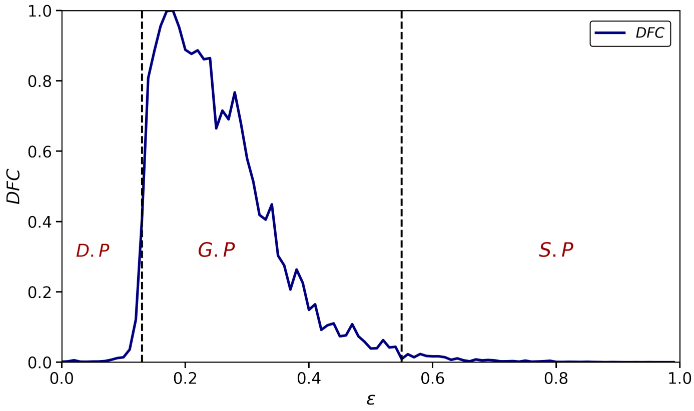

Figure 3.33: The plot showcases DFC in blue as a function of ϵ, spanning from 0 to 1. Calculations are based on a Small World Network of $N = 100$ nodes with p=0.038 and K = 40 (mean number of neighbours), each with a local parameter k_i in the range $[0.026, 0.03]$. DFC is averaged over 20 runs, omitting the first 10^5 steps. A bin size of 10^{-3} is used for DFC. acronyms D.P, G.P, and S.P stand for Desynchronization, Griffiths, and Synchronization Phases, respectively.

For each phase, an accompanying time series serves as evidence for its specific states.

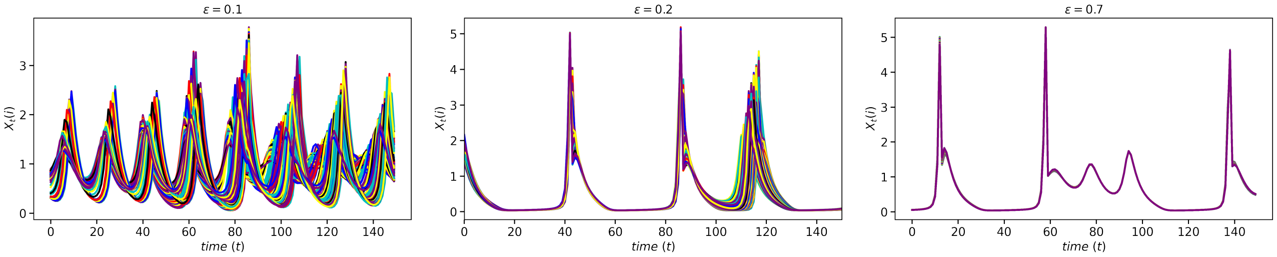

Figure 3.34: The time series of three distinct phases: the Desynchronization Phase at $\epsilon = 0.1$, the Griffith's Phase at the peak of DFC with $\epsilon = 0.2$, and Synchronization Phase at $\epsilon = 0.7$. All data are collected from a network of $N = 100$, $K = 40$ and $p = 0.038$ guided by Equations 3.5

As evident in Figure 3.34 with $\epsilon = 0.2$, the time series reveals a rich visual patterns. In the final analysis, let us take a closer look at some images that encapsulate this captivating phenomenon, where synchronization and desynchronization coexist spontaneously.

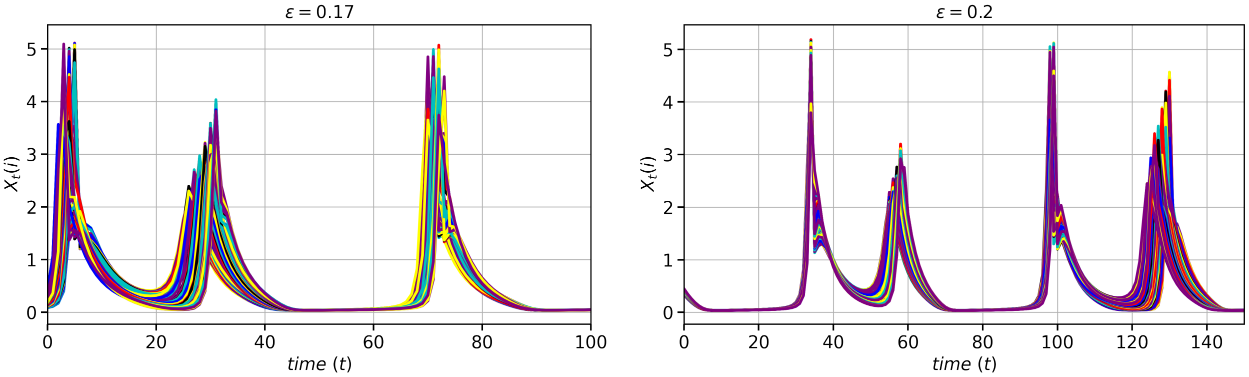

Figure 3.35: a) Time Series of $x(i)$: Sourced from a Small World Network with specifications $N = 100$, $K = 40$, and $p = 0.038$, as dictated by Equations 3.5. We consider k_i in the interval [0.026, 0.03] and exclude the first 10^5 transient steps. The coupling constant is $\epsilon = 0.17$. b) Similar to a), but uniquely differentiated by an interaction parameter $\epsilon = 0.2$ and a time frame of [0,100].

Chapter 4

Conclusions

Since its discovery by Shinoda and Kaneko in 2016, the phenomenon of chaotic Griffiths phase in dynamical networks remains not fully investigated and not well understood. In this state, the dynamical elements evolve repeatedly between the formation of synchronized clusters and desynchronization, where the size distribution of the synchronized clusters exhibits a power-law with a critical exponent. This behavior occurs on an continuous interval of a parameter, not just at a critical value as typical of second order phase transitions.

In this Thesis we have advanced the research into the chaotic Griffiths phase in coupled map networks. Our aim has been to elucidate the mechanisms that can produce this type collective behavior. We have extended Shinoda and Kaneko's work by exploring different local map dynamics and different topologies of the networks.

A main finding of the present work is the observation of a chaotic Griffiths phase in coupled map networks possessing neuron-based dynamics such as the Chialvo map. This results brings support to the conjecture that the chaotic Griffiths phase may explain the critical behavior reported in neural systems and the conscious brain as a dynamical process. The existence of parameter interval for critical behavior excludes the need for fine tuning of parameters thus facilitating the conscious functioning of the brain. In addition to the chaotic Griffiths phase, we have found complete synchronization and chimera states, where subsets of synchronized and incoherent elements coexist. These states have been associated to epilepsy pathology in the brain.

We have introduced the dispersion of the fraction of clusters (DFC) as a statistical quantity to characterize the chaotic Griffith phase in dynamical networks. We have shown that this measure is very successful in detecting the regions of parameters where a chaotic Griffiths phase occurs. As shown for the local logarithmic map, the dispersion of the fraction of clusters also serves to characterize intermittent behavior between synchronization and desynchronization.

We have found the chaotic Griffiths phase in random networks with different maps, indicating that the network heterogeneity is an scenario for the emergence of this phenomenon. By employing a heterogeneity measure, called asymmetry parameter, we have characterized the dispersion of the parameters of the local maps. We showed that heterogeneity in the local parameters can also induce the chaotic Griffiths phase. Thus, we have unveiled that the presence of heterogeneity in either the network topology or in the parameters of the dynamical elements, or in both, are mechanisms that can lead to the emergence of the chaotic Griffiths phase.

Besides the obvious need for more quantitative studies to elucidate the relation between the chaotic Griffiths phase and brain dynamics, many interesting questions arise from this Thesis as problems for future research. Are there other mechanisms that produce the chaotic Griffiths phase in dynamical networks? Does a chaotic Griffiths phase appear in continuous time dynamical systems, such as coupled Rössler oscillators? Can the chaotic Griffiths phase be studied in controlled experiments? Is there any mathematical formal relation between random topology (mechanism 1) and random heterogeneity in parameters (mechanism 2)? What is the relation between chaotic itinerancy and chaotic Griffiths Phase?

Bibliography

[1] Vojta, T. Rare region effects at classical, quantum and nonequilibrium phase transitions. *Journal of Physics A: Mathematical and General* **2006**, *39*, R143.

[2] Vazquez, F.; López, C.; Calabrese, J.; Munoz, M. A. Temporal Griffiths phase: a simple solution to the "savanna problem". **2009**,

[3] Parisi, G. *In a Flight of Starlings. The wonders of Complex Systems*; Publisher, 2022.

[4] Magazine, Q. Could One Physics Theory Unlock the Mysteries of the Brain? `https://www.youtube.com/watch?v=hjGFp7lMi9A`, 2023.

[5] Beggs, J. M.; Plenz, D. Neuronal avalanches in neocortical circuits. *J. Neurosci.* **2003**, *23*, 11167–11177.

[6] Shinoda, K.; Kaneko, K. Chaotic Griffiths Phase with Anomalous Lyapunov Spectra in Coupled Map Networks. *Physical Review Letters* **2016**, *117*, 254101.

[7] Watts, D. J.; Strogatz, S. H. Collective dynamics of ‘small-world’networks. *nature* **1998**, *393*, 440–442.

[8] Boccara, N. *Modeling complex systems*; Springer, 2010; Vol. 1.

[9] Kaneko, K.; Tsuda, I. *Complex Systems: Chaos and Beyond: A Constructive Approach With Applications in Life Sciences*; Springer Science & Business Media, 2001.

[10] Newman, M. E. *Networks: An Introduction*; Oxford University Press, 2012; 772 pages. ISBN-978-0-19-920665-0.

[11] Pikovsky, A.; Rosenblum, M.; Kurths, J. *Synchronization: A universal concept in nonlinear sciences*; Cambridge University Press, 2001.

[12] Dobson, I.; Carreras, B.; Lynch, V.; Newman, D. An initial model for complex dynamics in electric power system blackouts. 2001.

[13] Buldyrev, S. V.; Parshani, R.; Paul, G.; Stanley, H. E.; Havlin, S. Catastrophic cascade of failures in interdependent networks. *Nature (London)* **2010**, *464*, 1025.

[14] et al., M. N. Gene expression dynamics in the macrophage exhibit criticality. *Proc. Natl Acad. Sci. USA* **2008**, *105*, 1897–1900.

[15] Furusawa, C.; Kaneko, K. Adaptation to optimal cell growth through self-organized criticality. *Phys. Rev. Lett.* **2012**, *108*, 208103.

[16] Furusawa, C.; Kaneko, K. Adaptation to optimal cell growth through self-organized criticality. *Phys. Rev. Lett.* **2012**, *108*, 208103.

[17] Mora, T.; Bialek, W. Are biological systems poised at criticality? *J. Stat. Phys.* **2011**, *144*, 268.

[18] Shew, W. L.; Yang, H.; Petermann, T.; Roy, R.; Plenz, D. Neuronal avalanches imply maximum dynamic range in cortical networks at criticality. *The Journal of Neuroscience* **2009**, *29*, 15595–15600.

[19] Chialvo, D. R.; Bak, P. Learning from mistakes. *Physical Review Letters* **1999**, *90*, 1137–1148.

[20] Markovi ́c, D.; Gros, C. Power laws and self-organized criticality in theory and nature. *Physics Reports* **2014**, *536*, 41–74.

[21] Kaneko, K. Theory and Applications of Coupled Map Lattices. *Chaos* **1992**, Focus issue in Coupled Map Lattices.

[22] Jost, J.; Joy, M. P. Spectral properties and synchronization in coupled map lattices. *Phys. Rev. E* **2001**, *65*, 016201.

[23] Atay, F. M.; Jost, J.; Wende, A. Delays, Connection Topology, and Synchronization of Coupled Chaotic Maps. *Phys. Rev. Lett.* **2004**, *92*, 144101.

[24] Manrubia, S. C.; Mikhailov, A. S. Mutual synchronization and clustering in randomly coupled chaotic dynamical networks. *Phys. Rev. E* **1999**, *60*, 1579.

[25] Ito, J.; Kaneko, K. Spontaneous Structure Formation in a Network of Chaotic Units with Variable Connection Strengths. *Phys. Rev. Lett.* **2001**, *88*, 028701.

[26] Ito, J.; Kaneko, K. Spontaneous structure formation in a network of dynamic elements. *Phys. Rev. E* **2003**, *67*, 046226.

[27] Jalan, S.; Amritkar, R. E. Self-Organized and Driven Phase Synchronization in Coupled Maps. *Phys. Rev. Lett.* **2003**, *90*, 014101.

[28] Jalan, S.; Amritkar, R. E.; Hu, C. K. Synchronized clusters in coupled map networks. I. Numerical studies. *Phys. Rev. E* **2005**, *72*, 016211.

[29] Amritkar, R. E.; Jalan, S.; Hu, C. K. Synchronized clusters in coupled Map networks. II. Stability analysis. *Phys. Rev. E* **2005**, *72*, 016212.

[30] Griffiths, R. B. Nonanalytic behavior above the critical point in a random Ising ferromagnet. *Phys. Rev. Lett.* **1969**, *23*, 17–19.

[31] Petermann, T.; Thiagarajan, T. C.; Lebedev, M. A.; Nicolelis, M. A. L.; Chialvo, D. R.; Plenz, D. Spontaneous cortical activity in awake monkeys composed of neuronal avalanches. *Proc. Natl. Acad. Sci. U.S.A.* **2009**, *106*, 15921.

[32] Chialvo, D. R. Emergent complex neural dynamics. *Nature physics* **2010**, *6*, 744–750.

[33] Moretti, P.; Muñoz, M. A. Griffiths phases and the stretching of criticality in brain networks. *Nature communications* **2013**, *4*, 2521.

[34] Sato, K. First-order phase transition of a vacuum and the expansion of the Universe. *Monthly Notices of the Royal Astronomical Society* **1981**, *195*, 467–479.

[35] Beggs, J. M. *The cortex and the critical point: Understanding the power of emergence*; MIT Press, 2022.

[36] Cross, M.; Greenside, H. *Pattern formation and dynamics in nonequilibrium systems*; Cambridge University Press, 2009.

[37] Kadanoff, L. P. *Statistical physics: statics, dynamics and renormalization*; World Scientific, 2000.

[38] Wilson, K. G. Renormalization group and critical phenomena. I. Renormalization group and the Kadanoff scaling picture. *Physical review B* **1971**, *4*, 3174.

[39] Randeria, M.; Sethna, J. P.; Palmer, R. G. Low-Frequency Relaxation in Ising Spin-Glasses. *Physical Review Letters* **1985**, *54*, 1321–1324.

[40] Bray, A. J. Nature of the Griffiths phase. *Physical Review Letters* **1987**, *59*, 586–589.

[41] Noest, A. J. New universality for spatially disordered cellular automata and directed percolation. *Phys. Rev. Lett.* **1986**, *57*, 90–93.

[42] Munoz, M. A.; Juhász, R.; Castellano, C.; Ódor, G. Griffiths phases on complex networks. *Physical review letters* **2010**, *105*, 128701.

[43] Vazquez, F.; Bonachela, J. A.; López, C.; Munoz, M. A. Temporal griffiths phases. *Physical review letters* **2011**, *106*, 235702.

[44] Cota, W.; Ferreira, S. C.; Odor, G. Griffiths effects of the susceptible-infected-susceptible epidemic model on random power-law networks. *Physical review E* **2016**, *93*, 032322.

[45] Cota, W.; Ódor, G.; Ferreira, S. C. Griffiths phases in infinite-dimensional, non-hierarchical modular networks. *Scientific Reports* **2018**, *8*, 9144.

[46] Jr, E. G. L. The average lifetime of a population in a varying environment. *Journal of Theoretical Biology* **1981**, *90*, 213–239.

[47] Kamenev, A.; Meerson, B.; Shklovskii, B. How colored environmental noise affects population extinction. *Physical review letters* **2008**, *101*, 268103.

[48] Bialek, W. Perspectives on theory at the interface of physics and biology. *Reports on Progress in Physics* **2017**, *81*, 012601.

[49] Chen, X.; Dong, X.; Be'er, A.; Swinney, H.; Zhang, H. Scale-invariant correlations in dynamic bacterial clusters. *Phys. Rev. Lett.* **2012**, *108*, 148101.

[50] Bak, P. *how nature works*; na, 2002.

[51] Brunk, G. G. Why do societies collapse? A theory based on self-organized criticality. *Journal of Theoretical Politics* **2002**, *14*, 195–230.

[52] Munoz, M. A. Colloquium: Criticality and dynamical scaling in living systems. *Reviews of Modern Physics* **2018**, *90*, 031001.

[53] Mandelbrot, B. B. *The fractal geometry of nature*; Macmillan, 1983; Vol. 173.

[54] Newman, M. E. J. Contemp Phys 46 (5), 323, condmat/0412004. *Contemp Phys* **2005**, *46*, 323, condmat/0412004.

[55] Gisiger, T. Biol. Rev Cambridge Philosophical Soc.76 (02), 161. *Biol. Rev Cambridge Philosophical Soc.* **2001**, *76*, 161.

[56] Goldberger, A. L.; Amaral, L. A.; Hausdorff, J. M.; Ivanov, P. C.; Peng, C.-K.; Stanley, H. E. Proc. Natl. Acad. Sci. USA. 99 (suppl 1), 2466. *Proc. Natl. Acad. Sci. USA* **2002**, *99*, 2466.

[57] Bak, P.; Tang, C.; Wiesenfeld, K. Self-organized criticality: An explanation of the 1/f noise. *Physical review letters* **1987**, *59*, 381.

[58] Kandel, E.; Schwartz, J.; Jessel, T. *Principles of Neural Science*; McGraw-Hill, New York, 2000.

[59] Sporns, O. *Networks of the Brain*; MIT Press, USA, 2010.

[60] Fornito, A.; Zalesky, A.; Bullmore, E. *Fundamentals of brain network analysis*; Academic Press, 2016.

[61] Buendía, V.; Villegas, P.; Burioni, R.; Muñoz, M. A. The broad edge of synchronization: Griffiths effects and collective phenomena in brain networks. *Philosophical Transactions of the Royal Society A* **2022**, *380*, 20200424.

[62] Beggs, J. M. Phil Trans R Soc A 366 (1864), 329. *Phil Trans R Soc A* **2008**, *366*, 329.

[63] Cocchi, L.; Gollo, L. L.; Zalesky, A.; Breakspear, M. Progress in Neurobiology. *Progress in Neurobiology* **2017**,

[64] Hesse, J.; Gross, T. Front. Comput. Neurosci. 8. *Front. Comput. Neurosci.* **2014**, *8*.

[65] Plenz, D.; Niebur, E. *Criticality in neural systems*; John Wiley & Sons, 2014.

[66] Kitzbichler, M. G.; Smith, M. L.; Christensen, S. R.; Bullmore, E. Broadband criticality of human brain network synchronization. *PLoS Comput. Biol.* **2009**, *5*, e1000314.

[67] Shi, J.; Kirihara, K.; Tada, M.; Fujioka, M.; Usui, K.; Koshiyama, D.; ...,; Aihara, K. Criticality in the healthy brain. *Frontiers in Network Physiology* **2022**, *1*, 755685.

[68] Kinouchi, O.; Copelli, M. Optimal dynamical range of excitable networks at criticality. *Nature physics* **2006**, *2*, 348–351.

[69] Tagliazucchi, E.; Balenzuela, P.; Fraiman, D.; Chialvo, D. R. Criticality in large-scale brain fMRI dynamics unveiled by a novel point process analysis. *Front. Phys.* **2012**, *3*, 15.

[70] Sormunen, S.; Gross, T.; Saramäki, J. Critical drift in a neuro-inspired adaptive network. *Physical Review Letters* **2023**, *130*, 188401.

[71] Meunier, D.; Lambiotte, R.; Bullmore, E. T. Modular and hierarchically modular organization of brain networks. *Front. Neurosci.* **2010**, *4*, 200.

[72] Rubinov, M.; Sporns, O.; Thivierge, J. P.; Breakspear, M. Neurobiologically realistic determinants of self-organized criticality in networks of spiking neurons. *PLoS Comput. Biol.* **2011**, *7*, e1002038.

[73] Tagliazucchi, E.; Chialvo, D. R. The collective brain. *In Decision Making: A Psychophysics Application of Network Science* **2011**, 57–80.

[74] Chen, X.; Randi, F.; Leifer, A. M.; Bialek, W. Searching for collective behavior in a small brain. *Physical Review E* **2019**, *99*, 052418.

[75] Biswal, B.; Yetkin, F. Z.; Haughton, V. M.; Hyde, J. S. Functional connectivity in the motor cortex of resting human brain using echo-planar mri. *Magnetic resonance in medicine* **1995**, *34*, 537–541.

[76] Greicius, M. D.; Krasnow, B.; Reiss, A. L.; Menon, V. Functional connectivity in the resting brain: a network analysis of the default mode hypothesis. *Proc. Natl. Acad. Sci. USA* **2003**, *100*, 253–258.

[77] Tononi, G.; Sporns, O.; Edelman, G. M. A measure for brain complexity: relating functional segregation and integration in the nervous system. *Proc. Natl. Acad. Sci. USA* **1994**, *91*, 5033–5037.

[78] Villegas, P.; Hidalgo, J.; Moretti, P.; Muñoz, M. A. Frustrated hierarchical synchronization and emergent complexity in the human connectome network. *Sci. Rep.* **2014**, *4*, 5990.

[79] Villegas, P.; Hidalgo, J.; Moretti, P.; Muñoz, M. A. Complex synchronization patterns in the human connectome network. *In Proceedings of ECCS 2014* **2016**, 69–80.

[80] Strogatz, S. H. *Nonlinear dynamics and chaos with student solutions manual: With applications to physics, biology, chemistry, and engineering*; CRC press, 2018.

[81] Cosenza, M.; González, J. Synchronization and collective behavior in globally coupled logarithmic maps. *Progress of Theoretical Physics* **1998**, *100*, 21–38.

[82] Chialvo, D. R. Generic excitable dynamics on a two-dimensional map. *Chaos, Solitons & Fractals* **1995**, *5*, 461–479.

[83] Sánchez-Puig, F.; Zapata, O.; Pineda, O. K.; Iñiguez, G.; Gershenson, C. Heterogeneity extends criticality. *arXiv preprint arXiv:2208.06439* **2022**,

[84] Shibata, T.; Kaneko, K. Heterogeneity induced order in globally coupled chaotic systems. *Europhys. Lett.* **1997**, *38*, 417.

[85] Valdéz, A.; Cosenza, M. G. Comportamientos colectivos inducidos por diversidad en sistemas dinámicos espaciotemporales. *Revista Ciencia e Ingeniería* **2011**,

[86] Zhou, B.; Lu, X.; Holme, P. Universal evolution patterns of degree assortativity in social networks. *Social Networks* **2020**, *63*, 47–55.

[87] Ashby, W. R. *An Introduction to Cybernetics*; Chapman & Hall: London, 1956.

[88] Kaneko, K. From globally coupled maps to complex-systems biology. *Chaos: An Interdisciplinary Journal of Nonlinear Science* **2015**, *25*.

[89] Cano, A.; Cosenza, M. Chimeras and clusters in networks of hyperbolic chaotic oscillators. *Physical Review E* **2017**, *95*, 030202.

[90] Robalino, K. Collective behaviors induced by heterogeneity in dynamical networks. **2023**, To be published.

Appendices

Appendix A

Codes in Python

A.0.1 Power Law Clusters Counting

```
# Main Code
S_matrix = [[2, 1, 3],[1, 1.5, 4],[2.1, 0.1, 1.5, 2.1, 2.5, 2.7]]
data_0 = S_matrix
all_clusters=[]

for ij in range(len(data_0)):
    data= np.sort(data_0[ij])
    distance = np.abs(np.subtract.outer(data, data).T)
    arr2 = np.diag(distance, 1)
    connections = list(arr2)
    clusters_list = counting_clus(connections)
    all_clusters.extend(clusters_list)

# Clustering Function
def counting_clus(connections):
    delta = 0.5
    counts = []
    count = 0
    for num in connections:
        if num <= delta:
            count = count + 1
        else:
            if count > 0:
                counts.append(count + 1)
            count = 0
    if count > 0:
        counts.append(count + 1)
    return counts
```